Mechanical properties and deformation mechanisms of gradient nanostructured metals and alloys

Xiaoyan Li[1], *Lei Lu*[2], *Jianguo Li*[1], *Xuan Zhang*[1] *and Huajian Gao*[3,4]✉

Abstract | Inspired by the gradient structures of biological materials, researchers have explored compositional and structural gradients for about 40 years as an approach to enhance the properties of engineering materials, including metals and metallic alloys. The synthesis of various gradient nanostructured materials, such as gradient nanograined, nanolaminated nd nanotwinned metals and alloys, has provided new opportunities to understand gradient-related mechanical behaviour. These emerging gradient materials often exhibit unprecedented mechanical properties, such as strength–ductility synergy, extraordinary strain hardening, enhanced fracture and fatigue resistance, and remarkable resistance to wear and corrosion, which are not found in materials with homogeneous or random microstructures. This Review critically assesses the state of the art in the field of gradient nanostructured metallic materials, covering topics ranging from the fabrication and characterization of mechanical properties to underlying deformation mechanisms. We discuss various deformation behaviours induced by structural gradients, including stress and strain gradients, the accumulation and interaction of new dislocation structures, and unique interfacial behaviour, as well as providing insight into future directions for the development of gradient structured materials.

[1]*Center for Advanced Mechanics and Materials, Applied Mechanics Laboratory, Department of Engineering Mechanics, Tsinghua University, Beijing, China.*

[2]*Shenyang National Laboratory for Materials Science, Institute of Metal Research, Chinese Academy of Sciences, Shenyang, China.*

[3]*School of Mechanical and Aerospace Engineering, College of Engineering, Nanyang Technological University, Singapore, Singapore.*

[4]*Institute of High Performance Computing, A*STAR, Singapore, Singapore.*

✉*e-mail: huajian.gao@ntu.edu.sg*

https://doi.org/10.1038/s41578-020-0212-2

Many biological materials exhibit spatial gradients in the local chemical composition or constituents and/or structural characteristics[1]. Such spatial gradients improve the mechanical properties of biomaterials and endow functionality[1]. To optimize the mechanical properties and performance, chemical and/or structural gradients have been introduced into engineering materials[2–8] (FIG. 1). A spatial gradient in the microstructure and/or composition along a certain direction results in changes in the local or overall material properties. Notably, the introduction of a structural gradient can overcome traditional property trade-offs in conventional material systems, alleviate stress concentrations and give rise to specific functionalities. A gradient in the chemical composition leads to a gradient in properties associated with chemical bonding[1] and can be used to enhance various properties and functionalities of synthetic materials, including load bearing and support, impact damage resistance and interfacial toughening, as well as non-mechanical functions[1]. Chemical gradients have been studied mainly for biological materials[1]. For metals and alloys, structural gradients are more readily achieved and have attracted more attention in recent years.

From the 1980s to the 2000s, substantial effort was dedicated to fabricating functionally graded materials[2] — that is, a class of composites with graded patterns in the material composition and/or microstructure — with a primary focus on controlling the thermomechanical properties, such as thermal insulation. To date, the focus of functionally graded materials has been on high-temperature ceramics and Ti-based alloys. In the mid-2000s, gradient nanostructured (GNS) metals were introduced to overcome the strength–ductility trade-off of metallic materials[3–12]. GNS metals and alloys are typically designed with a gradient in the internal microstructure, such as grain size, twin thickness and/or lamellar thickness, from the surface to the interior (FIG. 1) over a characteristic length scale, ranging from several nanometres to hundreds of micrometres, or even to millimetres. The structural gradient results in a combination of mechanical properties that are superior to those of their coarse-grained (CG) counterparts and that include high strength, good ductility, high work hardening rate and improved fatigue resistance and friction properties[3–24]. In contrast to conventional homogeneous CG materials, a remarkable feature of GNS materials is that their deformation mechanism is often strongly heterogeneous, occurs progressively and successively, and is accommodated, intercoordinated and confined by the gradient microstructure. Furthermore, the structural gradient

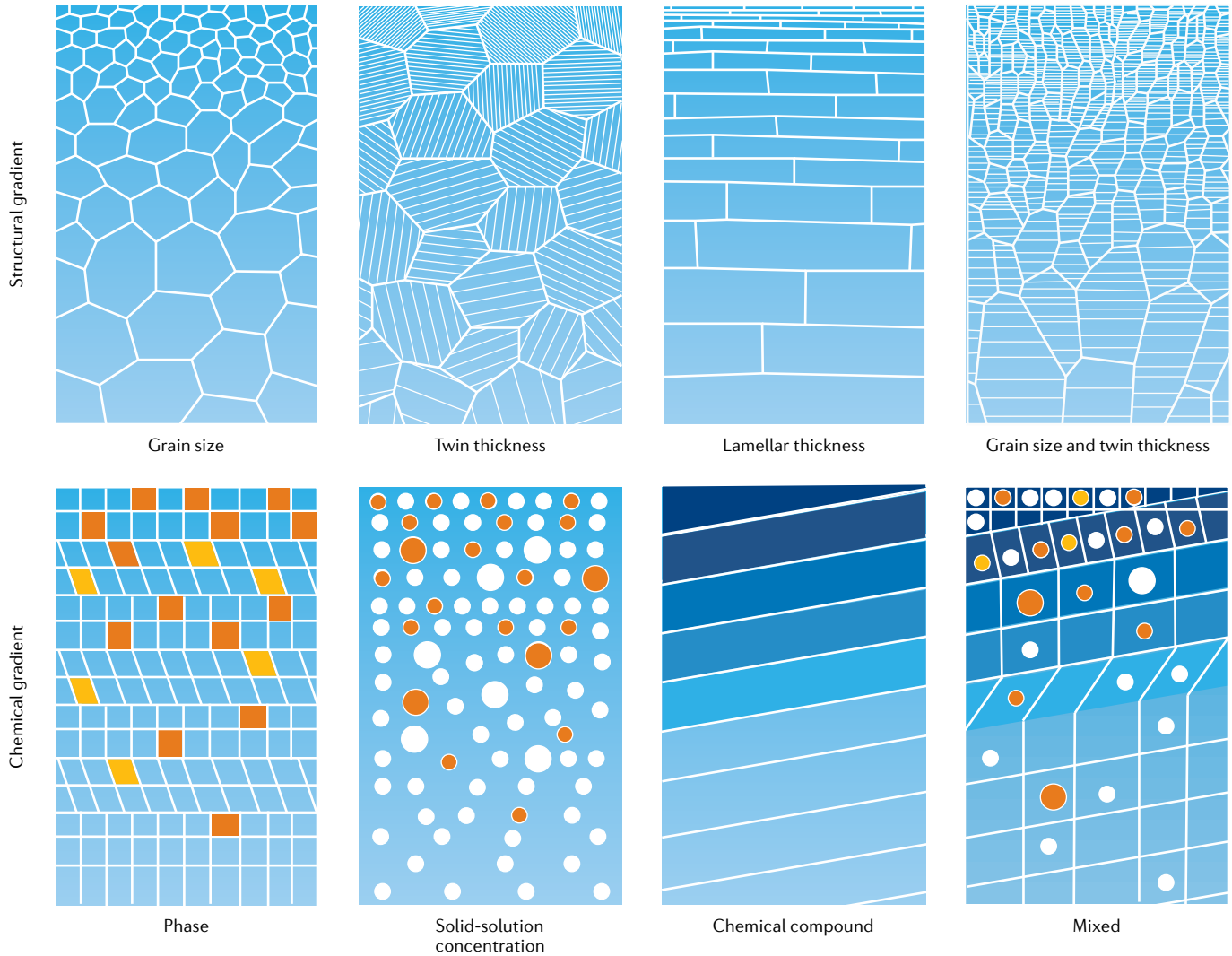

Fig. 1 | **Types of structural and chemical gradients in typical gradient materials.** Structural gradients include variations in the grain size, twin size and lamellar thickness. Chemical gradients include graded distributions in the phase, solid-solution concentration and chemical components. Some materials can have mixed structural and chemical gradients.

often induces stress and strain gradients and can even activate new dislocation structures in the material.

In this Review, we focus on the fabrication, microstructures, mechanical properties, fatigue and fracture performance, and deformation mechanisms of GNS metals and alloys. We discuss methods for synthesizing gradient nanograined, gradient nanolaminated and gradient nanotwinned metals and alloys, emphasizing the formation of a prevalent structural gradient in these materials. We summarize insight gained from experimental observations, conceptual and theoretical models, and multiscale simulations on the mechanical behaviour of GNS materials. Discussions on the deformation and failure mechanisms are accompanied by suggestions for tailoring high-performance GNS materials. We also review recent advances in the fundamental understanding of plastic deformation mechanisms in GNS metals and alloys and list open issues and challenges that need to be addressed for the design and fabrication of high-performance GNS materials.

Fabrication and microstructure

In this section, we review the typical fabrication and processing methods used to synthesize GNS metals and alloys, with emphasis on how the gradient structures form during fabrication, and highlight strategies for designing GNS materials. The fabrication methods can be classified into two categories: top-down approaches, including surface mechanical treatment methods[3,15,24–39], accumulative roll bonding[9,40,41] and laser shock peening[8,42–46], and bottom-up approaches, including physical and chemical deposition techniques, such as electrodeposition[7,13], magnetron sputtering[47] and 3D printing[48,49]. TABLE 1 summarizes the processing parameters, gradient thicknesses and sample types for various methods and processes used for fabricating GNS metals and alloys.

Surface mechanical treatment. Over the past two decades, three surface mechanical treatment methods have been developed to produce gradient nanostructures in a surface layer of bulk metallic materials: surface mechanical

attrition treatment (SMAT)[24–33], surface mechanical grinding treatment (SMGT)[3,34–38] and surface mechanical rolling treatment (SMRT)[15,39] (FIG. 2). During the SMAT process, the surface of the treated sample is impacted over a short period by many spherical steel shots with diameters of several millimetres (FIG. 2a), which are usually accelerated to high speeds by high-power ultrasound or other energy-transfer modes[27]. During the SMGT process, a hemispherical WC/Co tip penetrates tens of micrometres into a cylindrical sample that is rotating at high speed, and then slides along the axial direction of the sample at a relatively low speed (FIG. 2b). The SMRT process is similar to the SMGT process, with the main difference being that the tip in SMRT is a ball that rolls continuously under lubrication during sliding[15] (FIG. 2c).

Surface mechanical treatment methods induce severe plastic deformation, particularly a type of high-rate shear deformation, in the surface layer[3,15]. The strain rate near the top surface for SMAT can be as high as 10^2–$10^3\ s^{-1}$, whereas the strain rates for SMGT and SMRT[38] are ~10^3–$10^4\ s^{-1}$. The formation of gradient nanograined structures through surface mechanical treatment methods is due to plastic strain-induced grain refinement[50–52], which is related to the strain rate. During treatment, a large number of dislocations are generated and multiplied owing to severe plastic deformation. Subsequent interaction of these dislocations induces the formation of dislocation-cell walls, which gradually transform into sub-boundaries with small misorientations and further evolve into grain boundaries (GBs) with large misorientations as the applied strain accumulates[51]. These GBs separate an initial coarse grain into several fine grains with a mean grain size of ~100 nm (REF.[51]). Such grain refinement generally occurs in a subsurface layer of treated samples with low strain rates[51]. For metals and alloys with relatively low stacking fault energies, the grain subdivision often involves deformation twinning[50–52]. In this case, during severe plastic deformation, many nanoscale twins form owing to the low stacking fault energy and then divide the original coarse grains into twin-matrix lamellae[51,52]. The dislocation walls further subdivide the twin-matrix lamellae into equiaxed nanosized domains, which gradually evolve into randomly oriented nanograins with a minimum size of ~10 nm (REFS[51,52]). This grain refinement occurs at the top surface of treated samples under a high strain rate[51].

During surface treatment, there exists a gradient distribution of applied plastic strain and accumulated total plastic strain from the top surface to the interior. The extent of grain refinement is determined by the accumulation of applied plastic strain. Thus, a plastic strain gradient gives rise to a gradient distribution in the size of the refined grains. In metallic samples subjected to SMGT, the refined grains have different morphologies (such as equiaxed or laminated) and different types of GBs. Equiaxed grains with random misorientations are commonly produced, leading to the formation of the gradient nanograined structure in the treated surface layer. Recent experimental studies[35,38,39] have also reported the formation of gradient nanolaminated structures in the subsurface layer of Ni and Al. In these cases, many nanograins are elongated or extended along the rolling direction with a high density of low-angle GBs.

For gradient nanograined and gradient nanolaminated metals synthesized through SMGT, the grain size or lamellar thickness gradually increases from the top surface to the interior, and the local hardness of materials decreases with increasing grain size or lamellar thickness (FIG. 3a,b). Such a gradient structure is generated through a gradient in the plastic strain. There still exists a high density of dislocations in some grains (FIG. 3a,b, right parts), suggesting that the formation of a gradient nanograined structure is related to massive dislocation activities. Notably, SMGT and SMRT can be repeated several times to increase the thickness of the gradient layer by refining the grains during multiple treatment steps. Compared with SMAT, SMGT and SMRT produce a thicker and smoother gradient layer with increased

Table 1 | **Comparison of methods for fabricating GNS metals and alloys**

Fabrication method	Processing parameters	Gradient distribution or variation in feature size	Sample shape and type	Refs
SMAT	Diameter of spherical steel shots, impact velocity, impact time, environment	Tens of nanometres (top surface) to ~10 μm (interior)	Thin plates; metals and alloys	24–33
SMGT	Radius, rotation and sliding velocity, and penetration depth of WC/Co tip; treatment time, temperature	Several nanometres (top surface) to ~10 μm (interior)	Cylindrical bars; metals and alloys	3,34–38
SMRT	Radius, rotation and sliding or rolling velocity; penetration depth of tip, treatment time, temperature	Several nanometres (top surface) to ~10 μm (interior)	Cylindrical bars; metals and alloys	15,39
Accumulative roll bonding	Rotation velocity of rolls, thickness reduction, annealing temperature	Hundreds of nanometres (top surface) to ~1 μm (interior)	Thin plates; metals and alloys	9,40,41
Laser shock peening	Power, energy density and duration of laser, diameter of laser beam	Tens of nanometres (top surface) to ~100 nm (interior)	Complex geometrical shapes; metals and alloys	8,42–46
Electrodeposition, magnetron sputtering	Kinetics of deposition, current density, deposition power, chamber pressure	Tens of nanometres (top surface) to ~10 μm (interior)	Thin films or bulk; metals and alloys	7,13,47
3D printing	Size and followability of powders, power of electron-beam laser	Hundreds of nanometres (top surface) to ~10 μm (interior)	Printable shapes; metals and alloys	48,49

GNS, gradient nanostructured; SMAT, surface mechanical attrition treatment; SMGT, surface mechanical grinding treatment; SMRT, surface mechanical rolling treatment.

structural homogeneity[15]. During SMGT and SMRT, both the treated sample and the tip must be immersed in a cooling medium to suppress the unwanted rise in temperature[39], which can also influence grain evolution in the gradient layer.

Accumulative roll bonding. Accumulative roll bonding is a common technique for forming strong interfacial bonds between two or more layers of materials. Over the past 5 years, accumulative roll bonding has been used to fabricate various gradient nanolaminated metals and alloys[9,40,41]. During this process, plate samples are milled and compressed by two rotating rolls. In each rolling cycle, the sample thickness is reduced, and an additional shear deformation is simultaneously applied to induce grain refinement and even to form gradient structures, similarly to SMRT. As the number of rolling cycles increases, the grains become finer and the gradient layer becomes thicker. After rolling, the sample is annealed at high temperature to achieve partial recrystallization[9,40,41]. Compared with SMAT, SMGT and SMRT, accumulative roll bonding is more suitable for processing large-scale plate samples and industrial-scale production.

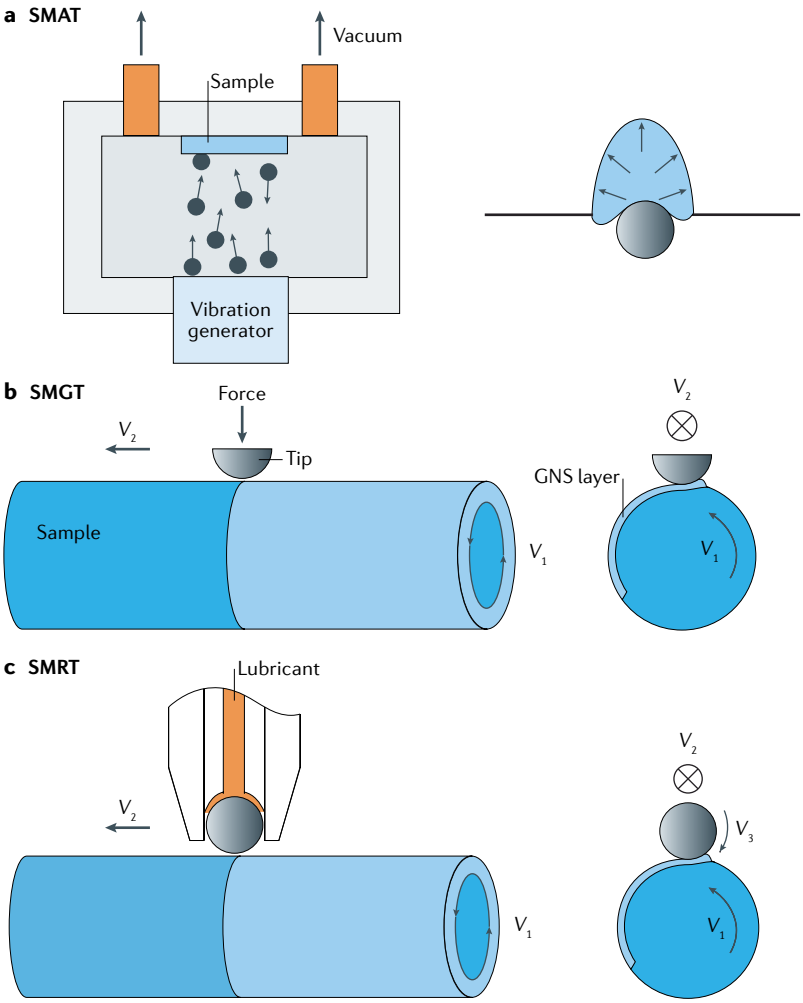

Fig. 2 | **Surface mechanical treatment methods. a** | Surface mechanical attrition treatment (SMAT) is used to treat plate-type samples[24]. Steel shots are accelerated to high speed and impact the sample. A close-up of the sample during processing is shown on the right. **b** | Surface mechanical grinding treatment (SMGT) is used to treat cylindrical samples[3]. A force is applied to a hemispherical tip, which penetrates into the rotating sample and slides along the axial direction. **c** | Surface mechanical rolling treatment (SMRT) is used to treat cylindrical samples[15]. Unlike SMGT, the tip is a lubricated ball that rolls continuously. V_1, V_2 and V_3 are the sample rotation, tip sliding and tip rolling speeds, respectively. GNS, gradient nanostructured. Panel **a** adapted with permission from REF.[27], Elsevier. Panel **b** adapted with permission from REF.[34], Elsevier. Panel **c** adapted with permission from REF.[15], Elsevier.

Laser shock peening. Laser shock peening is a commercial technique that is used to treat the surfaces of a wide variety of metallic components to increase their fatigue resistance[8,42–46]. This technique adapts a high-energy and ultrashort-duration (~10–30-ns) laser pulse to produce a compressive shock wave on the surface of treated materials. The shock wave carries a stress on the order of tens of gigapascals and induces heavy plastic deformation with an ultrahigh strain rate ($\sim 10^6\ s^{-1}$)[45]. After multiple shock peening impacts, initial coarse grains in the treated surface are divided into many fine grains through heavy plastic deformation. The laser-induced shock wave decays with depth, resulting in a surface layer with a gradient microstructure. Generally, the grain size increases from tens of nanometres (in the top surface layer of several micrometres) to hundreds of nanometres (interior). Occasionally, an amorphous layer with a thickness of ~10 nm forms at the top surface owing to ultrahigh compressive stress[44]. In addition to the gradient microstructure, a residual compressive stress is also introduced in the surface layer during laser shock peening[42–46]. This residual stress has a depth of hundreds of micrometres and can slow down the formation of fatigue cracks near the surface, helping to increase the fatigue life of treated samples.

Physical or chemical deposition. Physical or chemical deposition methods (including electrodeposition, magnetron sputtering and laser or electron-beam deposition) can be used to fabricate materials with accurate control of the microstructure through variation of the deposition kinetics and other parameters, such as temperature, current density and additive content. Various metals with gradient structures[7,13,47] have been synthesized by this approach. For example, gradient nanograined Ni plates were fabricated by continuous adjustment of the current density and additive content during electroplating deposition, with the average grain size varying from tens of nanometres to several micrometres along the thickness of the plate[13]. Gradient nanotwinned Cu samples were fabricated by a stepwise change of the electrolyte temperature of direct-current electrodeposition[13]. These samples exhibited a dual gradient in both grain size and twin thickness, with the average grain size increasing from 2.5 to 15.8 μm with depth and the average twin thickness simultaneously increasing from 29 to 72 nm (FIG. 3c). Gradient nanolaminated Cu–Zr samples were synthesized by alternate deposition of Cu and Zr through magnetron sputtering[47], with the lamellar thickness gradually increasing from 10 nm at the surface to 100 nm in the inner core. Moreover, with the rapid development of additive manufacturing, 3D printing based on laser or electron-beam deposition has been extended to fabricate various alloys with a gradient in composition[48]

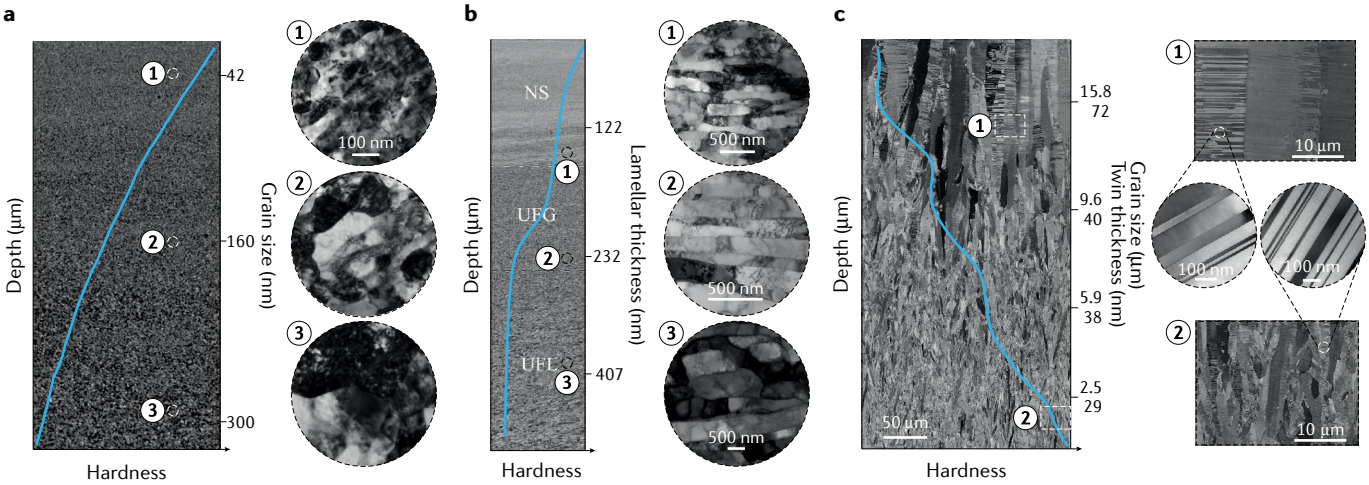

Fig. 3 | **Microstructure of gradient nanograined, gradient nanolaminated and gradient nanotwinned metals.** **a** | Scanning electron microscopy (SEM) image of gradient nanograined Cu showing that the grain size increases with depth. The close-ups are transmission electron microscopy (TEM) images of grains at different depths. **b** | SEM image of the microstructure in gradient nanolaminated Ni showing three distinct regions with nanostructures (NS), ultrafine-grained (UFG) and ultrafine-laminated (UFL) structures with increase of depth. The close-ups are TEM images of lamellae at different depths. **c** | SEM image of the microstructure of gradient nanotwinned Cu showing the decrease in grain size and twin thickness with depth. The close-ups are TEM images of grains and twins at different depths. The solid lines in each SEM image show the variation in local hardness with respect to depth in the gradient layer. Panel **a** adapted with permission from REF.[22], Elsevier. Panel **b** adapted with permission from REF.[38], Elsevier. Panel **c** adapted with permission from REF.[7], AAAS.

or phase size[49]. During 3D printing, a compositional gradient can be controlled by changing the volume fraction of a powder mixture[48], whereas a phase gradient can be introduced by tuning the cooling rate[49]. Compared with the other techniques mentioned above, the physical and chemical deposition methods have a major advantage for gradient nanostructures, because they typically enable precise control of the degree of gradient in the grain, twin and phase size, or composition. Thus, physical and chemical deposition is a feasible and promising method for designing and fabricating gradient metals and alloys with controllable gradient microstructures and desirable mechanical properties.

Mechanical properties

Most experimental studies have shown that GNS metals and alloys exhibit a unique combination of mechanical properties, including strength–ductility synergy[4,7,10,53–72], extraordinary work hardening[5,7,13,73–77], superior fatigue properties[14,16–19,78–91] and remarkable resistance to friction[20,92–95], wear[92–96] and corrosion[97–99]. These exceptional mechanical properties are closely linked to the gradient nanostructures of the materials.

Strength–ductility synergy. For conventional metals and alloys, strength and ductility are generally mutually exclusive[11], as illustrated by the so-called banana-shaped curve in FIG. 4a. Overcoming the strength–ductility trade-off is one of the major challenges for metallic materials[11]. Reducing the grain size to the nanoscale is an effective strategy to increase the strength of metals and alloys, because the GBs in nanocrystalline metals and alloys can effectively block dislocation motion[100]. However, grain-size reduction also results in a significant loss in ductility, owing to the constraint of plastic mechanisms inside small grains[100]. When the grain size is reduced to less than ~100 nm, the failure strain of nanocrystalline samples is typically reduced by an order of magnitude compared with that (usually >50%) of their CG counterparts[11,100] (FIG. 4a). Nanotwinned metals and alloys have been synthesized by introducing a high density of nanoscale twins into submicrometre-sized grains[101–107]. Compared with their CG counterparts, nanotwinned samples can achieve a yield strength that is several times higher at the cost of only slightly compromised ductility[102,108–111] (FIG. 4a). The ductility loss of nanotwinned samples is less than that of nanocrystalline samples as twin boundaries can accommodate and store a considerable number of mobile dislocations (such as threading dislocations and twinning partials)[109,110,112–116], which helps retain dislocation density while blocking dislocation motion. Numerous GNS metals and alloys[4,7,10,53–72] have been reported to have a desirable synergy of high strength and good ductility. The introduction of gradient nanostructures often leads to extra strengthening and hardening, corresponding to a synergetic effect that is greater than the sum of the individual effects. A few typical examples of GNS metals and alloys are discussed below.

A gradient nanograined Cu layer enclosing a CG core was recently fabricated by SMGT on a CG bar[3]. The grain size in the gradient layer varies from 20 to 300 nm over a depth of 150 μm, leading to a linear grain-size gradient of ~0.002. Such a structural gradient results in a depth gradient in local hardness as high as ~4.5 GPa mm^{-1} (FIG. 3a). The gradient nanograined layer leads to a doubling of strength without sacrificing tensile ductility. Moreover, the gradient nanograined

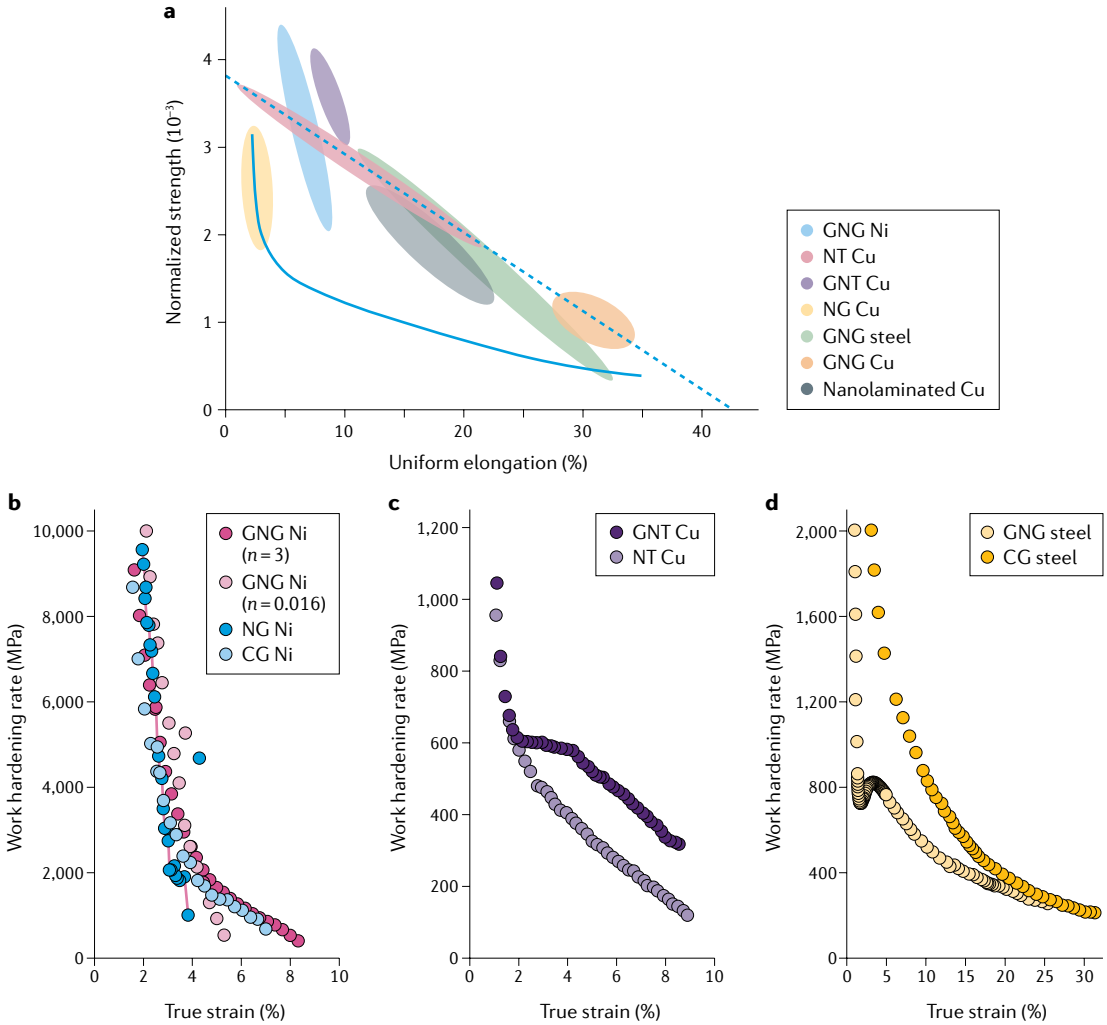

Fig. 4 | **Comparison of the mechanical properties of gradient nanostructured and homogeneous metals and alloys.** **a** | Normalized yield strength versus uniform elongation of various metals and alloys with nanograins, nanoscale twins and gradient nanostructures[7,13]. The banana-shaped solid curve indicates the strength–ductility trade-off of conventional metals and alloys, while the dashed line indicates the strength–ductility limit of current gradient nanograined (GNG), homogeneous nanotwinned (NT) and multilayered microstructures. **b** | Variation in work hardening rate with respect to true strain in coarse-grained (CG), nanograined (NG) and GNG Ni (REF.[13]). **c** | Variation in work hardening rate with respect to true strain in gradient nanotwinned (GNT) and NT Cu (REF.[7]). **d** | Variation in work hardening rate with respect to true strain in CG and GNG steels[5]. These plots indicate the strength–ductility synergy and extraordinary work hardening of gradient nanostructured metals and alloys. Panel **a** adapted with permission from REF.[13], Elsevier, and REF.[7], AAAS. Panel **b** adapted with permission from REF.[13], Elsevier. Panel **c** adapted with permission from REF.[7], AAAS. Panel **d** adapted with permission from REF.[5], PNAS.

layer can sustain a true tensile strain exceeding 100% without cracking when constrained by the CG core[3]. More recently, gradient nanograined Ni plates with controlled structural gradients have been prepared through electrodeposition[13]. The average grain size, d, at a position x along the thickness of the plate (the deposition direction) follows the relation[13]

$$d = d_{max} - (d_{max} - d_{min})(1 - x)^n, \quad (1)$$

where d_{min} and d_{max} denote the minimum and maximum values of d, respectively, and n is a power index that measures the degree of grain-size gradient. The greater the value of n, the larger the volume fraction of coarse grains and the smaller the volume fraction of fine grains. For all samples, d_{min} and d_{max} were set to 29 nm and 4 μm, respectively, while n was varied from 0.01 to 5 (REF.[13]). The grain-size gradient of the fabricated samples was as high as ~0.01, and the corresponding gradient in local hardness was ~5.0 GPa mm^{-1}. As the degree of gradient increases, the strength of the gradient samples decreases monotonically, whereas the range of uniform elongation first increases and then gradually decreases[13]. Compared with CG counterparts, gradient samples with $n = 3$–5 exhibit a higher yield strength and larger uniform elongation. Particularly, samples with $n = 3$ achieve an acceptable strength–ductility synergy. For gradient nanograined metals, grain coarsening or growth induced by GB migration dominates plastic deformation in the nanograins, whereas dislocation activities occur in the

coarse grains[3,13,22], indicating that the deformation is inhomogeneous in the overall material. The two distinct deformation mechanisms in the coarse grains and nanograins are mutually constrained and influenced, which helps to suppress strain localization in both the coarse grains and the nanograins, eventually leading to a combination of high strength and good ductility.

A gradient nanotwinned structure was obtained by subjecting a twinning-induced plasticity cylindrical steel bar to pretorsion of different angles[4]. The pretorsion produced a linear gradient distribution (in both thickness and density) of deformation twins along the radial direction of treated samples; that is, the volume fraction of twins and the average twin thickness increase nearly linearly with the radial distance from the centre to the surface[4]. The twin-size gradient was on the order of $\sim 10^{-5}$–10^{-4} and the local hardness gradient was as high as 0.5–2.0 GPa mm^{-1}. Transmission electron microscopy (TEM) revealed the formation and interaction of hierarchical nanoscale twins in all pretorsion-treated samples during subsequent tensile deformation. Similar hierarchical nanotwinned structures have been introduced in Cu (REF.[52]), Cu–Al alloys[117] and Cr–Co–Ni medium-entropy alloys[118] by surface treatment or pre-plastic deformation. Treated twinning-induced plasticity steels exhibit substantially higher strength and greater tensile ductility than untreated ones, which is attributed to the hierarchical nanoscale twins and their complex interaction with dislocations[4,52,117–119]. During tensile deformation, a network of secondary twins forms inclined to the primary twins formed during pretorsion treatment and penetrates through the latter. At the same time, some tertiary twins also form in the secondary twins, in directions parallel to the primary twins and then intersecting the secondary twins. The intersections between different-level twins lead to the formation of twin junctions, near which many dislocations accumulate. Recent large-scale atomistic simulations on the deformation of hierarchical nanotwinned metals[120–122] have revealed the interaction mechanisms between different-level twins and dislocations, with both strengthening and softening behaviours. Partial dislocations emitted from GBs or twin boundaries on inclined slip planes are blocked by different-level twin boundaries, contributing to the strengthening, whereas those nucleated from primary twin boundaries glide parallel to the secondary twin boundaries, leading to the detwinning of secondary twins. Together with the shifting of primary twin boundaries, the detwinning of secondary twins results in a softening behaviour with massive dislocation activities, maintaining good ductility.

Gradient nanotwinned Cu with a dual gradient in grain and twin sizes was fabricated by tuning of the electrolyte temperature during direct-current electrodeposition[7]. In the fabricated samples, the gradients in grain and twin sizes were up to ~0.03–0.15 and $\sim 2 \times 10^{-4}$–10^{-3}, respectively (FIG. 3c). The corresponding local hardness gradient varies from 1.75 to 11.6 GPa mm^{-1} (FIG. 3c). The strength of these gradient nanotwinned samples increases with the gradients in grain and twin sizes (or local hardness gradient) at the cost of slightly compromised uniform elongation[7]. Samples with the steepest structural gradient exhibited a combination of respectable ductility and strength higher than that of the strongest component of the gradient sample, which corresponds to a gradient-free nanotwinned material with a twin size equal to that of the smallest twin in the gradient sample[7]. The yield strength of a gradient nanotwinned sample is influenced by its gradient order[68]. Samples with a normal gradient order (hard surface and soft core) are stronger than those with a reverse gradient order (soft surface and hard core) because the normal gradient order helps suppress surface effects, leading to a higher strain gradient and stronger mutual constraint between the surface and the core during deformation[68]. Experimental observations and large-scale atomistic simulations revealed that the superior mechanical properties of dual-gradient nanotwinned metals originate from so-called bundles of concentrated dislocations (BCDs; discussed further below)[7], which is a dislocation structure that does not exist during deformation in homogeneous nanotwinned counterparts.

The variation in strength normalized by Young's modulus versus the uniform elongation of various metals and alloys with nanograins, nanoscale twins and gradient nanostructures is summarized in FIG. 4a. The results indicate that introducing gradient nanostructures is more effective than simply refining grains and introducing nanoscale twins for enhancing the material strength and persevering good ductility. Notably, some data for gradient nanograined Ni and gradient nanotwinned Cu are in otherwise unoccupied space (FIG. 4a), indicating that the gradient introduces an additional strengthening effect relative to homogeneous materials. This effect is associated with inhomogeneous deformation in gradient nanostructures. Both gradient nanograined Ni and gradient nanotwinned Cu have relatively large structural gradients (grain-size gradients of ≥0.01 and local hardness gradients >5.0 GPa mm^{-1}). Combined with experimental results[7,13] showing the influence of the grain-size and twin-size gradients on mechanical properties, it can be concluded that the distribution and degree of structural gradient are two key factors determining the mechanical properties of GNS metals and alloys. These results also suggest that regulating structural gradients in metallic materials can facilitate better strength–ductility synergy.

Work hardening. The work hardening (also known as strain hardening) of metallic materials is quantified by the work hardening rate, Θ, defined as $\Theta = d\sigma/d\varepsilon$, where σ and ε are the true stress and strain, respectively. The ductility of metallic materials is closely linked to their work hardening rate, which is governed by Hart's criterion[123–125] for the onset of plastic instability (mainly necking):

$$\Theta + m\sigma \leq \sigma, \tag{2}$$

where m denotes the strain-rate sensitivity of materials. For rate-insensitive materials (that is, $m = 0$), Eq. 2 is reduced to what is known as the Considère criterion of

necking[125]. To achieve good ductility in metallic materials, the onset of plastic instability must be postponed by averting the inequality in Eq. 2. Note that m is generally less than 0.05 for many metallic materials[11], in which case the work hardening rate has to be sufficiently high to sustain increasing stress[11]. Thus, on the basis of Hart's criterion, a high work hardening rate can ensure stabilized plastic deformation and good ductility.

Some GNS metals and alloys have exhibited extraordinary work hardening[5,7,13,73–77] (FIG. 4b,c). FIGURE 4b shows work hardening rates as a function of the true strain for CG, nanograined and gradient nanograined Ni (REF.[13]). The work hardening rate of nanograined samples declines more rapidly than that of CG samples as strain increases, leading to an earlier onset of plastic instability and reduced elongation (FIG. 4b). The work hardening rate of gradient nanograined samples depends on the degree of gradient[13], as quantified by the value of n in Eq. 1. Gradient samples with $n = 0.016$ show a variation in work hardening rate with strain that is similar to that of nanograined samples, signifying reduced ductility (FIG. 4b). However, compared with CG samples, gradient samples with $n = 3$ exhibit a higher work hardening rate in the initial stage of deformation and slower decay in the later stage, leading to higher strength and better ductility than CG samples with a mean grain size of 4 μm, as well as the largest elongation among the samples with different degrees of gradient[13]. Similarly to gradient nanograined metals, the work hardening rate of gradient nanotwinned Cu with a dual gradient[7] is higher than that of gradient-free nanotwinned Cu (FIG. 4c). After straining above 2%, the work hardening rate of gradient nanotwinned samples first experiences a plateau and then gradually decreases[7]. Such extraordinary work hardening stems from the formation of BCDs[7]. For gradient nanotwinned samples, the variation in work hardening rate with respect to strain appears to be dependent on the twin-size and grain-size gradients[7]. However, the detailed mechanism of this dependence remains unclear and needs to be studied further.

FIGURE 4d shows the variation in work hardening rate with respect to true strain for gradient nanograined steel and its CG counterpart. Although the gradient nanograined sample exhibits a quicker drop in the initial stage, a non-monotonic and transient hardening behaviour occurs at a small tensile strain of ~1.5%. Such an upturn in work hardening rate is not observed in CG and nanograined samples[5]. The upturn in the work hardening rate can be attributed to the nucleation and accumulation of dislocations under multiaxial stresses, which are activated by interactions between the CG core and the gradient layer[5], and to the generation of geometrically necessary dislocations (GNDs) caused by the grain-size gradient[5]. A similar upturn of work hardening rate was observed in gradient nanotwinned twinning-induced plasticity steels[4], but not in gradient-free counterparts. The mechanistic origin of this effect lies in the intersection between different-level twins and the accumulation of GNDs induced by the gradient twins[4]. After the upturn, the work hardening rate of gradient nanograined samples exhibits a slower decay than that of CG samples, leading to an extra strengthening effect in the former.

The work hardening rates of most fabricated GNS metals and alloys[7,13,73–77] are higher than those of gradient-free CG counterparts, especially in the later stage of plastic deformation. This work hardening behaviour enhances the strength and delays necking[74,75]. Such work hardening behaviour is inherent to gradient structures because it is associated with the formation of GNDs, which are needed to accommodate the strain gradient induced by gradient structures. Consequently, the work hardening capability of GNS metals and alloys can be tailored by tuning the structural gradient. Moreover, the temperature and the strain rate are two important parameters that regulate the work hardening of GNS metals and alloys. For metals with a low stacking fault energy, the working hardening rate of their GNS counterparts increases with decreasing temperature or increasing strain rate for reasons that seem to be related to the activation of deformation twinning and suppression of softening mechanisms under these conditions[75].

Fatigue. Fatigue is the most common failure mode of metallic materials in structural applications; however, enhancing the fatigue resistance of metallic materials is very challenging. Because fatigue cracks usually start from the surface of materials and then propagate into the interior during cyclic loading, strengthening the surface with nanostructures has been recognized as an effective strategy to protect materials against fatigue damage and failure[15,16,18]. Gradient nanostructures on the surface of materials can significantly enhance their fatigue resistance in both low-cycle and high-cycle fatigue regimes[14,16–19,78–91] (FIG. 5a,b).

Stress-controlled and strain-controlled tension–compression tests were performed to investigate the fatigue response of gradient nanograined metals and alloys[15,16,18]. The stress amplitude versus fatigue cycle curves of gradient nanograined Cu (with a gradient nanograined surface layer and a CG core) and homogeneous CG Cu from the stress-controlled and strain-controlled fatigue tests[18,19] are shown in FIG. 5a and FIG. 5b, respectively. The fatigue life of gradient nanograined samples is significantly longer than that of CG counterparts in the low-cycle and high-cycle fatigue regimes at the same strain and stress amplitudes. Notably, the fatigue endurance limit (that is, the stress amplitude at a fatigue life of more than 10^7 cycles) of gradient nanograined Cu reaches ~100 MPa, which is nearly twice that of a homogeneous CG sample[18]. A similar enhancement in the fatigue resistance of austenitic 316L stainless steels with a gradient nanograined surface layer was achieved in the high-cycle fatigue regime but not in the low-cycle fatigue regime[15]. TEM analyses showed that the enhanced fatigue resistance of gradient nanograined Cu is associated with fatigue-induced microstructural homogenization[16,18]. During the cyclic loading of gradient nanograined samples, grains continuously coarsen and grow owing to GB migration in the gradient nanograined surface layer, whereas grains in the CG core are gradually refined through the formation of intragranular dislocation cells[18,19]. Once the sizes of all grains in the gradient nanograined surface layer and CG core evolve to ~1 μm, the entire material turns into a structure with

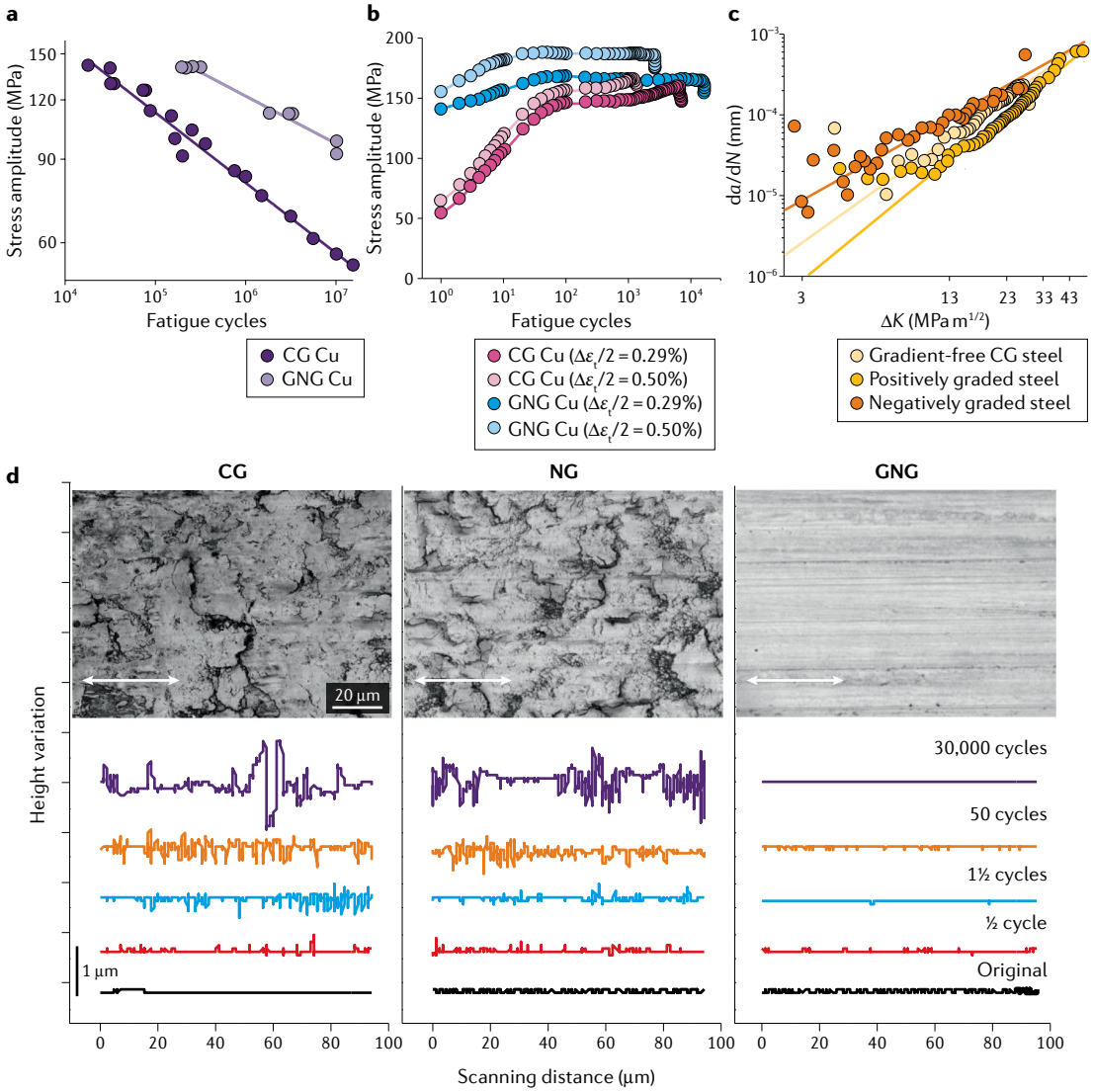

Fig. 5 | **Comparison of fatigue and friction behaviour in gradient nanostructured and homogeneous metals and alloys. a** | Dependence of high-cycle fatigue life on applied stress amplitude ($\Delta\sigma/2$, where σ is the stress) in gradient nanograined (GNG) and coarse-grained (CG) Cu (REF.[18]). **b** | Cyclic stress response ($\Delta\sigma/2$) at a total strain amplitude ($\Delta\varepsilon_t/2$) of 0.29% and 0.5% in GNG and CG Cu (REF.[18]). **c** | Fatigue crack growth rate (da/dN, where a is the crack length and N is the cycle number) as a function of the stress intensity factor range (ΔK) in gradient nanotwinned steels and CG steel[17]. **d** | Surface morphology of CG, nanograined (NG) and GNG Cu alloys after sliding. The top parts show confocal laser microscopy images of the surface morphologies after sliding for 18,000 cycles[20]. The bottom parts show the height profiles along the scanning direction indicated by the white arrows after different numbers of cycles. Panels **a** and **b** adapted with permission from REF.[18], Elsevier. Panel **c** adapted from REF.[17], CC-BY-4.0. Panel **d** adapted with permission of AAAS from REF.[20], © the Authors, some rights reserved; exclusive licensee American Association for the Advancement of Science. Distributed under a Creative Commons Attribution NonCommercial License 4.0.

homogeneous grains and then undergoes a steady-state cyclic response until eventual failure[18]. Two distinct deformation mechanisms in the gradient nanograined surface layer and CG core synergistically affect fatigue behaviour, suppressing the initiation of cracks and also accommodating large plastic strain, eventually resulting in enhanced fatigue resistance. During fatigue, grain coarsening first occurs in the subsurface layer and then propagates to the top surface[15,16,18]. Owing to accumulation of plastic strain at the top surface, fatigue cracks are nucleated from the top surface and then advance into the interior of gradient nanograined samples[15,16,18]. An increase in the volume fraction of the gradient nanograined surface layer enhanced the fatigue resistance of the overall sample, as the larger volume fraction of the gradient nanograined surface layer helps delay the expansion of grain coarsening from subsurface layers to the top surface[19].

For gradient nanograined metals and alloys fabricated through plastic deformation, and other surface treatment methods such as deep rolling and shot peening, a compressive residual stress is generated in gradient nanostructures during fabrication, owing to inhomogeneous plastic deformation in grains or between grains.

Gradient nanograined Cu exhibits a relatively longer fatigue life than in comparison with annealed gradient nanograined Cu with reduced residual stress in the surface gradient nanograined layer in the high-cycle regime[18,19]. This finding indicates that the existence of residual compressive stress in the gradient nanograined layer helps increase the high-cycle fatigue life of gradient nanograined Cu. The compressive residual stress can mitigate plastic strain accumulation in the gradient nanograined layer and arrest cracks or slow down crack propagation[18,19]. However, a few studies have demonstrated that large-amplitude cyclic straining in low-cycle fatigue tests may induce microstructure recovery, grain coarsening or microstructural homogenization in the overall sample and, thus, rapid release of residual stress in the gradient nanograined layer[15,16]. In this case, the influence of compressive stress on increasing low-cycle fatigue life of gradient nanograined metals may become negligible. However, the residual stress effect on microstructure evolution and cyclic properties of gradient nanograined metals and alloys in the low-cycle regime is still not entirely clear and needs further investigation.

Three-point bending tests on notched samples were conducted to characterize the fatigue behaviour and properties of gradient nanotwinned 304 austenitic steels prepared by pretorsion[17]. Two graded samples were used for the tests: one sample with a positive gradient (that is, the local hardness gradually increased with distance from the tip of the notch) and another sample with a negative gradient (that is, the local hardness gradually decreased with distance from the notch tip). FIGURE 5c shows the fatigue crack growth rate (da/dN, where a is the crack length and N is the cycle number) as a function of the stress intensity factor range (ΔK) for gradient nanotwinned samples with positive and negative gradients and, for comparison, gradient-free CG samples[17]. During steady-state fatigue crack propagation (that is, a regime with nearly linear dependence of da/dN on ΔK in the log–log plot), the positively graded sample has the lowest crack growth rate, followed successively by the gradient-free and negatively graded samples. These findings indicate that the positively graded sample exhibits the strongest resistance to fatigue crack growth, followed by the gradient-free sample and then the negatively graded sample. TEM revealed the underlying mechanisms behind this phenomenon: the positively graded sample has more twin and phase boundaries to block and confine the motion of dislocations along the path of crack propagation (that is, the direction of increasing twin density)[17]. Finite-element modelling of crack propagation further showed that the positively graded sample has both a smaller plastic zone and lower stress concentration in front of the crack tip than the other samples[17,89]. These results suggest that structural gradients can significantly alter the stress distribution and plastic zone size near a crack tip during fatigue crack propagation[17,89].

Friction, wear and corrosion. When metallic materials are subjected to dry sliding and wear, damage generally occurs at or near the surface owing to sliding-induced large plastic deformation underneath the surface, which could substantially shorten the service life of materials in practical applications. Therefore, it is crucial to improve the antifriction and antiwear properties of metallic materials. Some experimental studies[20,92–96] have shown that metallic materials with gradient nanograined surface layers exhibit lower friction coefficients and higher wear resistance than counterparts without gradient nanograined layers. After repeated sliding over 18,000 cycles, a large number of surface cracks, pile-ups and scars emerge at the surfaces of both CG and nanograined samples[20] (FIG. 5d, top). As the number of cycles increases, the surface roughness of CG and nanograined samples increases dramatically. However, for gradient nanograined samples, no cracks or pile-ups are detected, and no change in surface roughness is observed during 30,000 cycles[20] (FIG. 5d, bottom). The steady-state fiction coefficient of samples with a gradient nanograined surface layer is only 0.29 under high loads, which is much lower than that (~0.60–0.68) of nanograined and CG samples[20]. TEM observations and finite-element modelling[20,95] revealed that the underlying mechanisms responsible for the superior antifriction and antiwear properties are related to the high work hardening capability of the gradient nanogradient layer, which can accommodate large plastic deformation through grain coarsening, suppressing surface roughening and delamination of the tribolayer[20,95,96]. The gradient nanograined surface layer should be sufficiently thick (approximately hundreds of micrometres) to resist high-cycle friction and wear under high loads. Otherwise, after a certain number of cycles, the gradient nanograined layer undergoes delamination as a result of surface cracks and subsequently wears away, resulting in an abrupt decrease in friction and wear resistance[92]. In particular, the surface of some metals readily oxidizes in air and then mixes mechanically with unoxidized parts to form a mechanically mixed surface layer during sliding[92]. Such a mechanically mixed surface layer can undergo delamination during subsequent cyclic sliding[92], leading to poorer antifriction and antiwear properties.

When the gradient nanograined surface layer is produced by treating the surface of metallic materials through severe plastic deformation, a compressive residual stress is usually introduced into the gradient nanograined layer. The magnitude of the residual stress can be estimated by comparing the load–displacement curves of indentation between gradient nanograined and untreated gradient-free samples[93]. The residual stress at the topmost surface is usually on the order of ~100 MPa (REF.[93]). With increasing depth from the topmost surface, the residual stress decreases gradually. Compressive residual stress in the gradient nanograined sample can delay crack initiation (compared with gradient-free samples) and reduce crack propagation velocity after crack nucleation[93,96]. These findings indicate that compressive residual stress can considerably improve the antifriction and antiwear properties of materials.

In contrast to friction and wear, there have been relatively few studies[97–99] on the influence of a gradient nanograined layer on the corrosion behaviour of metallic materials. Experimental studies[97–99] have shown that 304 and 316 stainless steels treated by SMAT exhibited

lower corrosion resistance at room temperature than untreated samples. The reason for this is that SMAT induces the formation of surface defects and an increase in strain energy in the surface layer, which prevents the formation of passivation films, leading to degradation in the corrosion resistance of the material[97]. However, if these samples are subsequently treated by annealing or nitriding, the corrosion resistance can be increased[98,99] owing to grain growth and the release of strain energy. When SMAT is used to treat Ni-based alloy 690, the gradient nanograined layer formed during SMAT provides diffusion paths for Cr, promoting rapid formation of a dense protective oxide layer, thereby enhancing corrosion resistance at high temperature[99]. The aforementioned studies show that the gradient nanograined layer formed by SMAT does not always have a beneficial effect on corrosion resistance. The influence of a gradient nanograined layer on the corrosion behaviour of metallic materials depends on the material type, the SMAT processing parameters, the SMAT-induced surface defects and the environmental temperature[126]. Currently, the effect of a gradient nanograined layer on corrosion is poorly understood and requires further, and more systematic, study.

Deformation mechanisms

During the deformation of GNS metals and alloys, the structural gradient induces a plastic deformation incompatibility that is generally accommodated through the generation of GNDs[11,21,73,127,128], which further leads to a plastic strain gradient and a stress gradient. This inhomogeneous deformation on the scale of the structural gradient is fundamentally different from deformation in conventional metallic materials. In particular, some novel dislocation activities, interface-related behaviour and interactions between GNDs and interfaces have been observed. Moreover, a long-range heterodeformation-induced stress field develops[11,73,129,130] from the inhomogeneous deformation of gradient nanostructures. In this section, we discuss the deformation mechanisms responsible for the mechanical properties of GNS metals and alloys, with the aim of building connections between mechanical properties, deformation mechanisms and the microstructure. Furthermore, the relationship between the structural gradient and the deformation gradient is highlighted, and theoretical models of GNDs and heterodeformation-induced stress are also reviewed.

Plastic strain gradient. Owing to the presence of a grain-size gradient and the dependence of yield strength on grain size, the plastic deformation in gradient nanograined metals and alloys progressively propagates from the soft CG core to the hard nanograined layer[3,11], inducing a deformation gradient (FIG. 6a–c). This deformation gradient has been verified through crystal plasticity finite-element modelling[21,60] of 2D and 3D gradient nanograined samples. Plots of the distributions of tensile stress and plastic strain (FIG. 6d,e) over the cross section of a 2D gradient nanograined sample demonstrate gradients in both stress and plastic strain. The plastic strain is larger in the CG core and smaller in the top and bottom surface layers (FIG. 6e). Three-dimensional gradient nanograined samples exhibited more pronounced strain gradients than 2D samples in the late stage of plastic deformation[60] owing to greater deformability in all three directions. Finite-element modelling[21,60] also showed a tensile stress gradient in the gradient nanograined samples during plastic deformation, with larger stress at the top and bottom surfaces and smaller stress in the CG core (FIG. 6d), which is opposite the distribution of a plastic strain gradient. Experimentally measured height profiles on the lateral surface normal to the tensile direction of gradient nanograined steels with a gradient nanograined layer and a CG core[5] showed that the absolute value of the lateral strain gradually increases from the CG core to the surface layer, indicating the presence of a plastic strain gradient in the gradient nanograined layer. Such a stress and/or strain gradient is generated owing to the structural gradient in gradient nanograined samples under uniaxial tension, which is a uniform deformation. The strain gradient of gradient nanograined samples under uniaxial tension is different from strain-gradient plasticity induced by applying a non-uniform deformation (such as bending[131], torsion[132] or indentation[133]). However, both phenomena — that is, strain gradients induced by either a structural gradient or a non-uniform deformation — involve inhomogeneous deformation.

A theoretical model[134] showed that when metallic materials undergo inhomogeneous deformation, the resulting deformation gradient and incompatibility can be accommodated by GNDs with density ρ_G, which is related to the strain gradient by[134]

$$\rho_G = \frac{1}{b}\frac{\partial \gamma}{\partial x}, \tag{3}$$

where b is the magnitude of the Burgers vector of the GNDs and γ the shear strain due to dislocation slip. Equation 3 indicates that the density of GNDs is directly linked to the strain gradient. For a conventional polycrystal under uniaxial tension, the density of GNDs in a grain that accommodates the deformation incompatibility between neighbouring grains can be roughly estimated as[134]

$$\rho_G = \frac{\bar{\varepsilon}}{4bD}, \tag{4}$$

where D is the grain size and $\bar{\varepsilon}$ is the plastic strain. For plastically deformed gradient nanograined samples, GNDs are similarly generated near GBs to accommodate the deformation incompatibility between neighbouring grains (FIG. 6f). According to Eq. 4, the density of GNDs in gradient nanograined samples depends on both the grain size and the plastic strain gradient[11]. Existing strain-gradient plasticity theories[134–136] indicate that the inhomogeneous deformation related to GNDs induces non-local strengthening. Therefore, it can be speculated that GNDs induced by the structural gradient significantly contribute to the strengthening of gradient nanograined samples. Experiments on gradient nanograined steels[5] verified this speculation and showed

that the accumulation and interaction of GNDs have an important role in the observed strengthening and extraordinary work hardening of gradient nanograined samples. For nanograined samples, quantitative relationships between the structural gradient, strain gradient and GND distribution are still unknown. Therefore, to model the deformation of gradient nanograined samples, it will be necessary to develop a new modelling framework that incorporates quantitative relationships between these parameters. The development of new models could be crucial for designing gradient nanograined materials and optimizing their mechanical properties and performance.

Recently, large-scale atomistic simulations[137] were conducted on the uniaxial tension of gradient nanograined Cu with grain-size gradients varying from 0 to 0.42.

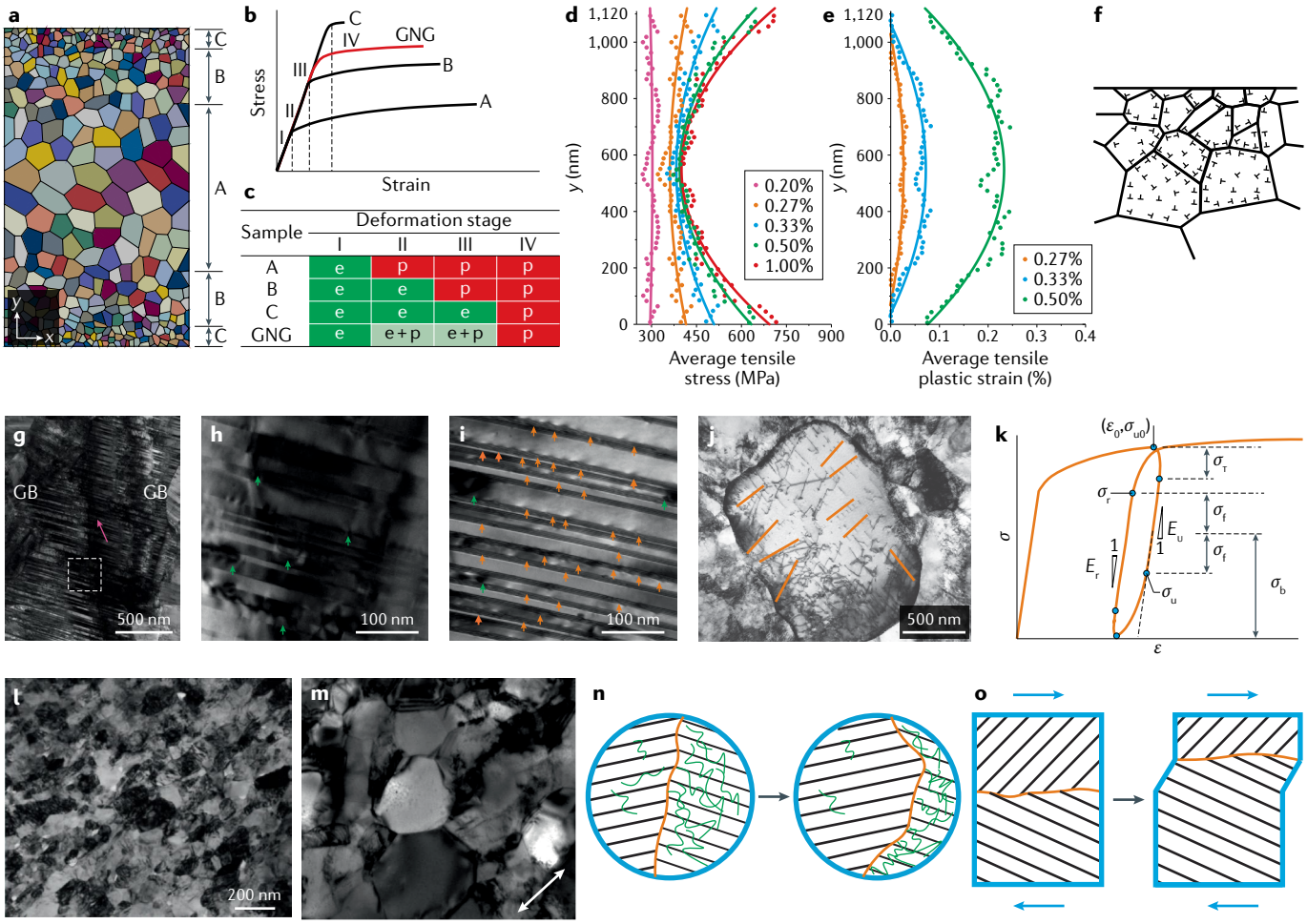

Fig. 6 | **Deformation mechanisms in gradient nanostructured metals and alloys. a** | Model of a gradient nanograined (GNG) structure comprising components A, B and C; the grain size increases from the top and bottom to the centre. **b** | Tensile stress–strain curves of a GNG metal and its components A, B and C showing progressive yielding of the components in four typical deformation stages, I, II, III and IV. **c** | Evolution of the strain of components A, B and C in a GNG metal from stage I to stage IV in panel **b**. 'e' and 'p' represent elastic and plastic strain, respectively. 'e + p' represents the coexistence of both elastic and plastic strain. **d**,**e** | Distribution of axial tensile stress and plastic strain in the cross section of 2D GNG Cu at various applied strains calculated by finite-element modelling of the sample under uniaxial tension[21]. The results indicate that the stress and plastic strain gradients originate from the grain-size gradient and show the progressive development of gradient stress and plastic strain fields. **f** | Illustration of the distribution of geometrically necessary dislocations (GNDs; represented by ⊥ near the grain boundaries (GBs)) in a plastically deformed GNG structure[21]. **g** | Transmission electron microscopy (TEM) image of deformed gradient nanotwinned Cu with a dual gradient in the grain and twin sizes[7]. A bundle of concentrated dislocations is indicated by the red arrow. **h**,**i** | TEM images of the region in the white square in panel **g**, identified by two-beam diffraction[7] using vectors of $\mathbf{g}_M = \mathbf{g}_T = 111$ (panel **h**) and $\mathbf{g}_M = 200$ (panel **i**). $\mathbf{g}_M$ and $\mathbf{g}_T$ are the diffraction vectors used in the matrix and twin domains for TEM observations, respectively. Mode I and mode II dislocations are indicated by the green and orange arrows, respectively. **j** | TEM image showing dislocation pile-ups (orange lines) in front of a GB in a large grain in a heterogeneous lamellar structure[54]. **k** | Stress (σ)–strain (ε) unloading–reloading loop of a GNG sample[12], where σ_f is the frictional stress, σ_b is the back stress, σ_u is the unloading yield stress, σ_r is the reloading yield stress, σ_T is the thermal stress, σ_{u0} and ε_0 are the initial flow stress and strain at the beginning of unloading, and E_u and E_r are the unloading and reloading moduli. **l**,**m** | TEM images of the top surface of GNG Cu at different tensile strains of 5% (panel **l**) and 25% (panels **m**) at room temperature[22] indicating homogeneous grain coarsening due to GB migration under plastic deformation. The arrow in part **m** indicates the tensile direction. **n** | GB bulging. **o** | GB migration coupled with shear deformation (the blue arrows indicate the shear direction). Panels **a**, **d**–**f** adapted with permission from REF.[21], Elsevier. Panels **g**–**i** adapted with permission from REF.[7], AAAS. Panel **j** adapted with permission from REF.[54], PNAS. Panel **k** adapted with permission from REF.[12], CC-BY-4.0. Panels **l** and **m** adapted with permission from REF.[22], Elsevier.

These simulations showed that there exists a critical average grain size for the onset of strength softening and that this critical size decreases with increasing grain-size gradient[137]. The emergence of a critical size arises from the combined effect of GB sliding and migration in smaller grains and enhanced intergranular dislocation activities in larger grains[137]. The atomistic simulations also demonstrated the presence of a plastic strain gradient and stress gradient during plastic deformation, and the storage of GNDs to coordinate the deformation between neighbouring small and large grains[137].

Unique dislocation structures. Over the past few years, nanolaminated composites with two immiscible metals (such as Ag–Cu, Cu–Nb, Cu–Ni and Al–Ag) arranged in alternating layers have been fabricated by various deposition techniques[138–142]. The thicknesses of the nanolayers of these composites range from several nanometres to hundreds of nanometres[138–142]. Owing to the immiscibility of the two metals, there is a high density of coherent or incoherent bimetal interfaces in the nanolaminated composites[138–142]. In addition to the bimetal interfaces, a high density of nanoscale twins exists in the grain interiors of the constituent metal with the lower stacking fault energy. During deformation of these nanolaminated composites, the interactions between dislocations, bimetal interfaces and nanoscale twins result in ultrahigh hardness and strength[143,144]. In contrast to metallic nanolaminated composites with homogeneous layer thicknesses, gradient nanolaminated samples with alternating soft Cu and hard Zr nanolayers fabricated by magnetron sputtering possess high strength and could undergo large coupled deformation (with a maximum uniform layer strain of 60%)[47]. The coupled deformation can be accounted for by the accumulation of GNDs near the interlayer interfaces, which accommodate strain incompatibility between the Cu and Zr layers with a gradient in the thickness[47]. Laminated structures with alternating CG Cu layers and nanostructured Cu–10wt% Zn layers[40,63] exhibited high work hardening and remarkable tensile ductility, surpassing values predicted by the rule of mixtures. These unique mechanical responses have been attributed to abundant GNDs nucleating from interfacial ledges and piling up near neighbouring interfaces[63], resulting in the formation of an interface-affected zone. Such an interface-affected zone was confirmed by in situ high-resolution strain mapping near the interlayer interfaces[63]. The width of a zone depends on the applied strain with an approximate magnitude of several micrometres[63]. The laminated samples achieve optimal strength–ductility synergy when neighbouring interface-affected zones start to overlap[63].

In homogeneous nanotwinned metals, there are three typical dislocation activities[108–111,127]: dislocations slip inclined to twin boundaries; threading dislocations are confined by neighbouring twin boundaries; and partial dislocations glide along twin boundaries, leading to detwinning. The first and second dislocation activities are hardening mechanisms (called hard mode I and hard mode II, respectively), whereas the third one is a softening mechanism (called soft mode III). In gradient nanotwinned metals with a dual gradient[7], a new dislocation structure — the BCD (that is, a bundle assembly of ultrahigh-density dislocations) — was observed to govern plastic deformation (FIG. 6g). The detailed structure of a BCD was revealed by a two-beam diffraction technique in TEM[7] (FIG. 6h,i). A BCD contains both mode I and mode II dislocations, with the density of mode II dislocations nearly one order of magnitude higher than that of mode I dislocations[7]. Atomistic simulations[7] produced nearly the same structure of BCDs and further revealed that BCDs also carry several stair-rod dislocations. This BCD structure is essentially a type of GND because it is generated to accommodate strain gradient induced by the dual gradients in grain size and twin size. The accumulation and interaction of BCDs, which are uniformly distributed in the grain interior, not only induce strengthening but also facilitate delocalization of plastic deformation[7], leading to high strength and good ductility.

Heterodeformation-induced stress. During plastic deformation of GNS metals and alloys, many GNDs are generated to accommodate the plastic strain gradient induced by the gradient nanostructures[5,12,21]. According to existing strain-gradient plasticity theory[145–149], when GNDs accumulate or pile up on a slip system against interfaces or barriers (as exemplified by the dislocation pile-ups in front of the GB in FIG. 6j), a long-range stress is produced owing to the self-stress and interaction of the GNDs[145–149]. This long-range stress obstructs further slip of mobile dislocations[145] and is often referred to as a 'back stress'. If we consider only the self-stress of GNDs with a continuous distribution of GND density, ρ_G, the back stress, σ_b, on a slip system scales as[24,149]

$$\sigma_b \propto \mu b R^2 \frac{\partial \rho_G}{\partial x}, \tag{5}$$

where μ is the shear modulus, and R is the domain radius for GNDs contributing to the back stress, which is generally on the same order of magnitude as the length scale of the GND distribution[149]. A combination of Eqs 3 and 5 indicates that the back stress is essentially associated with a second-order strain gradient[149].

The additional strengthening and extraordinary work hardening of gradient nanograined metals and alloys has been accounted for by considering the effect of back stress from GNDs[12,24]. Owing to the physical origin of back stress, it can be measured by analysing the unloading–reloading stress–strain hysteresis loop (FIG. 6k) of gradient nanograined samples under uniaxial tension[12]. During loading and unloading, only the frictional stress, σ_f, from the lattice and the back stress are considered. This analysis assumes that the frictional stress remains constant throughout the unloading–reloading process, whereas the back stress is unchanged before the yield point of unloading[12] (FIG. 6k). The unloading yield stress $\sigma_u = \sigma_b - \sigma_f$ at the unloading yield point in FIG. 6k, and the reloading yield stress $\sigma_r = \sigma_b + \sigma_f$ at the reloading yield point[12] in FIG. 6k. Thus, if we combine the expressions for σ_u and σ_r, $\sigma_b = (\sigma_r + \sigma_u)/2$. Replacing σ_r with the initial flow stress at the beginning of unloading, σ_{u0}, further

eliminates the effect of thermal stress, σ_T, and eventually the following expression is obtained[12]:

$$\sigma_b = \frac{\sigma_{u0} + \sigma_u}{2} - \frac{\sigma_T}{2}. \quad (6)$$

Analysis of experimentally measured unloading–reloading stress–strain loops of gradient nanograined samples using Eq. 6 revealed that the back stress is as large as ~30–50% of the yield and flow stresses[12]. The back stress gradually increases with increasing applied strain[12], suggesting that as the applied strain increases, an increasing number of GNDs accumulate, leading to higher back stress. Moreover, the findings revealed that gradient nanograined samples have higher back stress than their CG counterparts during plastic deformation[12]. In particular, in the upturn regime of the work hardening rate[5], the increasing rates of back stress with respect to strain in the gradient nanograined samples are much higher than those in CG samples[12]. These results indicate that the back stress has a crucial role in enhancing the strength and work hardening of gradient nanograined samples. Similar analyses of the effect and contribution of back stress can be extended to other GNS materials and, more generally, to heterogeneous structured materials (such as materials with harmonic, domain-dispersed, hierarchical and mixed nanostructures)[11,73].

Most recently, it was proposed that the pile-up of GNDs produces the back stress in the soft domains, which in turn induces the forward stress in the hard domains[130]. The back and forward stresses are thought to be coupled long-range internal stresses in opposite directions[130]. The back stress makes the soft domain stronger, but the forward stress makes the hard domain weaker, as both domains deform plastically, especially when the soft domain is constrained by the hard domain[130]. Therefore, the coupling of back and forward stresses increases the global yield strength and contributes to the extra hardening of gradient nanograined metals and alloys[130]. The back and forward stresses are related to heterogeneous deformation[130] and can collectively be referred to as the 'heterodeformation-induced stress'[130].

Grain coarsening. During plastic deformation of gradient nanograined metals and alloys, two distinct deformation mechanisms are observed[3,16,18,19,22,23]: grain coarsening or growth, which operates in the gradient nanograined layer, and conventional dislocation activities, which occur in the CG cores. These two deformation mechanisms synergistically contribute to a combination of high strength and good ductility of gradient nanograined samples[3,22]. During the uniaxial tension of gradient nanograined samples, grain coarsening occurs gradually and homogeneously as the applied strain increases and dominates plastic deformation in the gradient nanograined layer[3,22] (FIG. 6l,m). During cyclic fatigue tests, grain coarsening always starts from an ultrafine-grained subsurface layer and gradually extends to the top surface with increasing cycles until all grains in the gradient nanograined layer attain the same size[16,18,19,23]. Grain coarsening is a strain-softening mechanism[3,22,127], because the flow stress of materials gradually decreases with increasing grain size. However, grain coarsening can accommodate large plastic strain and help to suppress shear localization or instability in the gradient nanograined layer, thus contributing to good ductility and high fatigue resistance[3,16,18,19,22,23].

The grain coarsening in the gradient nanograined layer is induced by GB migration. Grain coarsening can occur at high stress levels and cryogenic temperatures[22]. This realization implies that GB migration is driven by mechanical loads rather than by a diffusional process[3,22]. There are two common mechanisms for mechanically driven GB migration, which might be operative during grain coarsening in the gradient nanograined layer (FIG. 6n,o). If two neighbouring grains have different dislocation densities, their shared GB can move by absorbing dislocations and bulging into the grain with a higher dislocation density (FIG. 6n). The driving force of this GB migration is the internal strain energy stored in the dislocations (including dislocation core energy). As the GB migrates, the strain energy in the grain with the higher dislocation density is gradually released, and the area swept by the GB becomes free of dislocations. When a GB migrates along its normal direction under shear stress, it couples with a shear of the lattice traversed by the GB (FIG. 6o). This coupled GB migration, driven by an applied shear stress, has been confirmed by experiments and atomistic simulations[150–152]. The results from these studies also revealed that low-angle and high-angle tilting GBs exhibit high mobility through the coupled GB migration mechanism[151]. During GB migration, the motion of low-angle tilting GBs is achieved by the collective motion of the array of dislocations that constitute such GBs, whereas that of high-angle tilting GBs is accomplished by the deformation of constituent structural units[151]. It is well recognized that GB migration is determined mainly by the structure, energy, misorientation and chemical composition of GBs, as well as external factors, including stress, temperature and strain rate[153]. A recent study on the uniaxial tension of gradient nanograined metals[154] reported that GB migration is also dependent on the initial grain size. As the initial grain size decreases from the submicrometre level, GB migration first intensifies and then gradually weakens[154]. Consequently, there is a critical grain size that corresponds to the strongest GB migration. The weakening of GB migration below a critical grain size can be ascribed to GB relaxation during sample processing or post-heat-treatment[154]. This realization suggests that, even in gradient nanograined metals, very small nanosized grains can stabilize the structure providing the GBs are substantially relaxed[154].

Connections between mechanisms. There are connections between the various plastic deformation mechanisms experimentally observed in GNS metals and alloys and the mechanical properties and microstructures. The deformation mechanisms include plastic strain gradients due to progressive yielding, unique dislocation activities (essentially activities of GNDs), heterodeformation-induced long-range stress (mainly back stress) and grain coarsening induced by GB migration. All of these deformation mechanisms originate

from the structural gradients of GNS metals and alloys, and contribute to their mechanical properties. Grain coarsening occurs in the gradient layer of gradient nanograined metals and is related to GB migration. Both plastic strain gradient and heterodeformation-induced stress occur in all GNS metals and alloys, and can be attributed to the generation and accumulation of GNDs during plastic deformation. GNDs and the resultant strain gradient and internal stress are important features of plastic deformation of GNS metals and alloys. Currently, nearly all theoretical and computational modelling at the microscale, mesoscale and macroscale for plastic deformation of GNS metals and alloys is based on the strain-gradient plasticity. A thorough understanding of plastic deformation in metallic GNS materials requires further development of more advanced theoretical frameworks and computational modelling techniques.

Future perspectives

As an emerging class of nanostructured materials, GNS metals and alloys have achieved a combination of excellent mechanical properties that are not always possible in their homogeneous counterparts. These mechanical properties originate from the gradient microstructures, wherein a host of inhomogeneous plastic deformation mechanisms are activated involving multiple deformation features and mechanisms, including pronounced strain gradients, novel dislocation activities and mechanically driven grain coarsening. Although some advances in the fabrication and mechanics of GNS metals and alloys have been made, there are numerous crucial issues that need to be addressed. Here we highlight some key open issues and challenges (FIG. 7) for the further development and innovation of GNS materials.

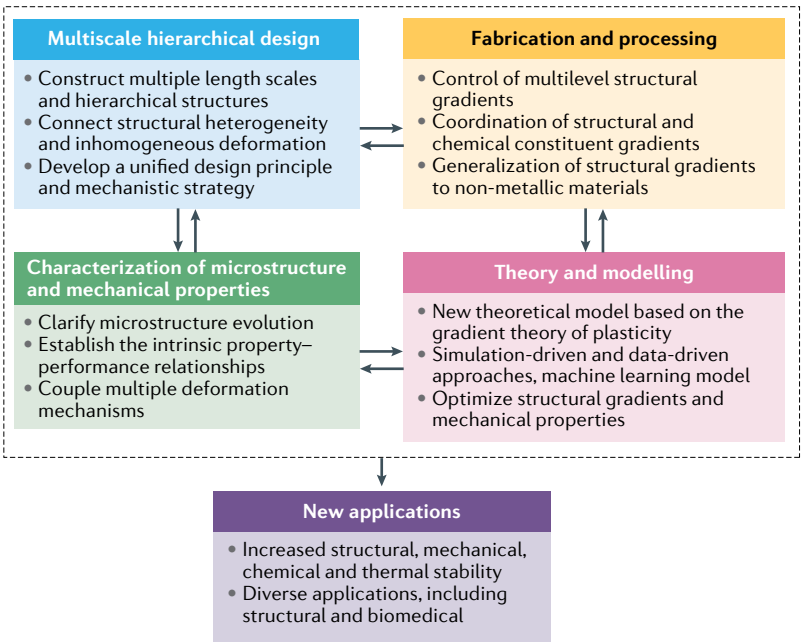

Fig. 7 | **Open issues and challenges for gradient nanostructured metals and alloys.** Inspired by the rapid development of this field in recent years, we summarize the issues and challenges in the development of gradient nanostructured materials. Some issues are also applicable to heterogeneous nanostructured materials more generally.

Theory, modelling and design. As the relationship between structural gradients and mechanical properties in GNS materials remains mostly qualitative, current design and optimization of gradient nanostructures are largely empirical. It has become urgent to develop theoretical and computational modelling frameworks to quantify correlations between microstructural gradients (such as the degree and distribution of structural gradients and variations in the dimensions and orientations of building blocks) and the mechanical properties of GNS materials. Although it is known that the mechanical properties of GNS materials are strongly determined by their structural gradients, it remains a challenge to design gradients to achieve optimal mechanical properties. In recent years, simulation-driven and data-driven approaches have expedited and simplified material design and discovery processes[155–158]. In particular, machine learning models trained with experimental and simulation data have been used to predict material structures and properties to determine the structure–property relationships and guide material design and synthesis[155,156,158]. Owing to the current lack of quantitative theoretical models for GNS materials, we anticipate major advances in the coming decade in the development of machine learning approaches to designing and optimizing structural gradients to achieve targeted mechanical properties.

Fabrication and processing. Current processing techniques for GNS materials cannot precisely control structural gradients from the nanoscale to the macroscale. Therefore, the degree and distribution of gradients in synthetic GNS materials generally fall in a very limited range. By contrast, naturally occurring gradients in biological materials span multiple length scales and hierarchical structures. Precise control of multilevel structural gradients over a wide range of length scales and replication of the hierarchical structures in natural biomaterials requires the development of new fabrication processes. Moreover, current GNS metals and alloys are limited to a few pure face-centred-cubic metals and typical alloys. It can be anticipated that similar principles of structural gradients can be extended to many more metallic and non-metallic systems, and that structural gradients will increasingly be combined with other gradients, such as compositional gradients, in the design of gradient materials.

Microstructure and mechanics. Inhomogeneous deformation in GNS materials involves multiple deformation mechanisms and intricate internal stress and strain states induced by the structural gradient over different length scales. To advance the fundamental understanding of GNS materials, it will be essential to fully clarify the complicated evolution of the microstructure, related to the interactions between dislocations, boundaries and interfaces, as well as the origin, coupling and trade-offs of different mechanisms and internal stresses and strains across multiple length scales. To address these issues, more systematic and detailed microstructural characterization and mechanical studies need to be conducted with the help of multiscale modelling and theoretical

studies. Current experimental methods cannot effectively characterize the coupling of multiple deformation mechanisms and internal stress and/or strains across multiple length scales, as most methods cannot integrate information over multiple scales and instead deal with only individual mechanisms at a given scale. Therefore, more advanced and effective experimental methods (especially those with the capability of in situ characterization) need to be developed to explore the mutual influence between various deformation mechanisms and internal stress and strains, and to evaluate their contributions to the mechanical response of GNS materials. Furthermore, most experimental studies to date have focused mainly on the plastic deformation of GNS metals and alloys under monotonic loading. Revealing the fatigue, fracture and creep behaviour and the associated failure mechanisms of GNS metals and alloys will be essential to fully explore their engineering applications. For example, the influence of residual stress on the fatigue, fracture and creep behaviour of GNS materials remains to be clarified. Moreover, the mechanical properties and deformation mechanisms at low or high temperature and corrosion behaviour in different environments are also some of the issues for future investigation.

Multiscale and hierarchical structures. For natural biomaterials, structural gradients often exhibit hierarchical features and diverse chemical gradients spanning multiple length scales[1], resulting in excellent mechanical properties and multiple functionalities. Such gradients in biomaterials provide inspiration for designing and fabricating GNS materials with unprecedented properties and performance. Therefore, how to design, construct and control multiple length scales and hierarchical structures in GNS materials to achieve targeted properties and performance is an important question. GNS metals and alloys can be regarded as a type of heterogeneously structured material. The family of heterogeneously nanostructured materials has expanded in recent years, with materials with harmonic, domain-dispersed, hierarchical and mixed nanostructures[11,73,159,160] having emerged under various structural and architectural designs[11]. These materials have a high strain hardening capability and often evade the strength–ductility trade-off. For example, nanoscale domains with a mean grain size of ~7 nm and a small misorientation of <15° were found to spread through ultrafine-grained Ni, forming unique domain-dispersed nanostructures[160]. These nanostructures lead to both high strength and a high strain hardening rate, as well as good ductility[160]. Inspired by the recent advances and successes in the development of GNS metals and alloys, we anticipate that a unified design principle and mechanistic strategy may soon emerge for these more general heterogeneously structured materials, and that the connections between complex structural heterogeneity and inhomogeneous deformation will be exploited to enhance mechanical properties.

New applications of GNS materials. The unique gradient nanostructures endow GNS metals and alloys with remarkable mechanical properties. The high strength and high resistance to crack propagation of these materials make them suitable for safety-critical applications and load-bearing structural applications in, for example, the aerospace, automobile, microelectronics and sporting industries. Similar structural gradients can be introduced in GNS ceramics and ceramic composites for applications as dental and orthopaedic implants. Combined with the intrinsic multifunctionality of metals and alloys, it will be interesting to explore applications of GNS metals and alloys in interdisciplinary fields, including tribology, geology, optoelectronics[161], biomechanics and nanotechnology. However, the limited long-term structural, mechanical, chemical and thermal stabilities of these materials are issues that must first be addressed. Moreover, integrated studies that explore coupled physical and chemical properties of GNS metals and alloys are required for realization of applications.

Published online: 08 July 2020

1. Liu, Z., Meyers, M. A., Zhang, Z. & Ritchie, R. O. Functional gradients and heterogeneities in biological materials: design principles, functions, and bioinspired applications. *Prog. Mater. Sci.* **88**, 467–498 (2017).
2. Suresh, S. Graded materials for resistance to contact deformation and damage. *Science* **292**, 2447–2451 (2001).
3. Fang, T., Tao, N. & Lu, K. Revealing extraordinary intrinsic tensile plasticity in gradient nano-grained copper. *Science* **331**, 1587–1590 (2011).
An early experimental report on gradient nanograined metals with extraordinary mechanical properties.
4. Wei, Y. et al. Evading the strength–ductility trade-off dilemma in steel through gradient hierarchical nanotwins. *Nat. Commun.* **5**, 3580 (2014).
5. Wu, X., Jiang, P., Chen, L., Yuan, F. & Zhu, Y. T. Extraordinary strain hardening by gradient structure. *Proc. Natl Acad. Sci. USA* **111**, 7197–7201 (2014).
6. Thevamaran, R. et al. Dynamic creation and evolution of gradient nanostructure in single-crystal metallic microcubes. *Science* **354**, 312–316 (2016).
7. Cheng, Z., Zhou, H., Lu, Q., Gao, H. & Lu, L. Extra strengthening and work hardening in gradient nanotwinned metals. *Science* **362**, eaau1925 (2018).
An early experimental report on gradient nanotwinned metals with extraordinary mechanical properties.
8. Zhao, S. et al. Generating gradient germanium nanostructures by shock-induced amorphization and crystallization. *Proc. Natl Acad. Sci. USA* **114**, 9791–9796 (2017).
9. Ma, X. et al. Mechanical properties of copper/bronze laminates: role of interfaces. *Acta Mater.* **116**, 43–52 (2016).
10. Wu, X. et al. Synergetic strengthening by gradient structure. *Mater. Res. Lett.* **2**, 185–191 (2014).
11. Ma, E. & Zhu, T. Towards strength–ductility synergy through the design of heterogeneous nanostructures in metals. *Mater. Today* **20**, 323–331 (2017).
12. Yang, M., Pan, Y., Yuan, F., Zhu, Y. T. & Wu, X. Back stress strengthening and strain hardening in gradient structure. *Mater. Res. Lett.* **4**, 145–151 (2016).
13. Lin, Y., Pan, J., Zhou, H., Gao, H. & Li, Y. Mechanical properties and optimal grain size distribution profile of gradient grained nickel. *Acta Mater.* **153**, 279–289 (2018).
14. Roland, T., Retraint, D., Lu, K. & Lu, J. Fatigue life improvement through surface nanostructuring of stainless steel by means of surface mechanical attrition treatment. *Scr. Mater.* **54**, 1949–1954 (2006).
An early experimental study on enhancing fatigue properties of steel with a gradient nanograined surface layer.
15. Huang, H. W., Wang, Z. B., Lu, J. & Lu, K. Fatigue behaviors of AISI 316L stainless steel with a gradient nanostructured surface layer. *Acta Mater.* **87**, 150–160 (2015).
16. Yang, L., Tao, N., Lu, K. & Lu, L. Enhanced fatigue resistance of Cu with a gradient nanograined surface layer. *Scr. Mater.* **68**, 801–804 (2013).
17. Ma, Z. et al. Strength gradient enhances fatigue resistance of steels. *Sci. Rep.* **6**, 22156 (2016).
18. Long, L. et al. Improved fatigue resistance of gradient nanograined Cu. *Acta Mater.* **166**, 56–66 (2019).
A recent experimental study on enhancing fatigue properties of gradient nanograined Cu.
19. Jing, L., Pan, Q., Long, J., Tao, N. & Lu, L. Effect of volume fraction of gradient nanograined layer on high-cycle fatigue behavior of Cu. *Scr. Mater.* **161**, 74–77 (2019).
20. Chen, X., Han, Z., Li, X. & Lu, K. Lowering coefficient of friction in Cu alloys with stable gradient nanostructures. *Sci. Adv.* **2**, e1601942 (2016).
An experimental study on lowering the coefficient of friction in Cu alloys with a gradient nanograined surface layer.
21. Zeng, Z. et al. Gradient plasticity in gradient nano-grained metals. *Extreme Mech. Lett.* **8**, 213–219 (2016).
22. Chen, W., You, Z., Tao, N., Jin, Z. & Lu, L. Mechanically-induced grain coarsening in gradient nano-grained copper. *Acta Mater.* **125**, 255–264 (2017).

23. Long, J., Pan, Q., Tao, N. & Lu, L. Abnormal grain coarsening in cyclically deformed gradient nanograined Cu. *Scr. Mater.* **145**, 99–103 (2018).
24. Li, J., Weng, G., Chen, S. & Wu, X. On strain hardening mechanism in gradient nanostructures. *Int. J. Plast.* **88**, 89–107 (2017).
25. Lu, K. & Lu, J. Surface nanocrystallization (SNC) of metallic materials-presentation of the concept behind a new approach. *J. Mater. Sci. Technol.* **15**, 193–197 (1999).
26. Wu, X. et al. Microstructure and evolution of mechanically-induced ultrafine grain in surface layer of Al-alloy subjected to USSP. *Acta Mater.* **50**, 2075–2084 (2002).
27. Lu, K. & Lu, J. Nanostructured surface layer on metallic materials induced by surface mechanical attrition treatment. *Mater. Sci. Eng. A* **375**, 38–45 (2004).
28. Zhu, K. Y., Vassel, A., Brisset, F., Lu, K. & Lu, J. Nanostructure formation mechanism of α-titanium using SMAT. *Acta Mater.* **52**, 4101–4110 (2005).
29. Roland, T., Retraint, D., Lu, K. & Lu, J. Enhanced mechanical behavior of a nanocrystallised stainless steel and its thermal stability. *Mater. Sci. Eng. A* **445**, 281–288 (2007).
30. Chen, A. Y. et al. The influence of strain rate on the microstructure transition of 304 stainless steel. *Acta Mater.* **59**, 3697–3709 (2011).
31. Yang, D. K., Cizek, P., Fabijanic, D., Wang, J. T. & Hodgson, P. D. Work hardening in ultrafine-grained titanium: multilayering and grading. *Acta Mater.* **61**, 2840–2852 (2013).
32. Hassani-Gangaraj, S. M., Cho, K. S., Voigt, H. J. L., Guagliano, M. & Schuh, C. A. Experimental assessment and simulation of surface nanocrystallization by severe shot peening. *Acta Mater.* **97**, 105–115 (2015).
33. Meng, X. C. et al. The deformation behavior of AZ31 Mg alloy with surface mechanical attrition treatment. *Mater. Sci. Eng. A* **707**, 636–646 (2017).
34. Li, W. L., Tao, N. R. & Lu, K. Fabrication of a gradient nano-micro-structured surface layer on bulk copper by means of a surface mechanical grinding treatment. *Scr. Mater.* **59**, 546–549 (2008).
35. Liu, X. C., Zhang, H. W. & Lu, K. Strain-induced ultrahard and ultrastable nanolaminated structure in nickel. *Science* **342**, 337–340 (2013).
36. Wang, H. T., Tao, N. R. & Lu, K. Architectured surface layer with a gradient nanotwinned structure in a Fe–Mn austenitic steel. *Scr. Mater.* **68**, 22–27 (2013).
37. Liu, X. C., Zhang, H. W. & Lu, K. Formation of nanolaminated structure in an interstitial-free steel. *Scr. Mater.* **95**, 54–57 (2015).
38. Liu, X. C., Zhang, H. W. & Lu, K. Formation of nano-laminated structure in nickel by means of surface mechanical grinding treatment. *Acta Mater.* **96**, 24–36 (2015).
39. Xu, W., Liu, X. C. & Lu, K. Strain-induced microstructure refinement in pure Al below 100 nm in size. *Acta Mater.* **152**, 138–147 (2018).
40. Ma, X. L. et al. Strain hardening and ductility in a coarse-grain/nanostructure laminate material. *Scr. Mater.* **103**, 57–60 (2015).
41. Zhang, L. et al. Fabricating interstitial-free steel with simultaneous high strength and good ductility with homogeneous layer and lamella structure. *Scr. Mater.* **141**, 111–114 (2017).
42. Nalla, R. K. et al. On the influence of mechanical surface treatments — deep rolling and laser shock peening — on the fatigue behavior of Ti–6Al–4V at ambient and elevated temperatures. *Mater. Sci. Eng. A* **355**, 216–230 (2003).
43. Ye, C., Liao, Y. L., Suslov, S., Lin, D. & Cheng, G. J. Ultrahigh dense and gradient nano-precipitates generated by warm laser shock peening for combination of high strength and ductility. *Mater. Sci. Eng. A* **609**, 195–203 (2014).
44. Luo, S. H. et al. Surface nanocrystallization of metallic alloys with different stacking fault energy induced by laser shock processing. *Mater. Des.* **104**, 320–326 (2016).
45. Ren, X. D. et al. Microstructure evolution and grain refinement of Ti-6Al-4V alloy by laser shock processing. *Appl. Surf. Sci.* **363**, 44–49 (2016).
46. Laine, S. J., Knowles, K. M., Doorbar, P. J., Cutts, R. D. & Rugg, D. Microstructural characterisation of metallic shot peened and laser shock peened Ti-6Al-4V. *Acta Mater.* **123**, 350–361 (2017).
47. Li, J. J. et al. Eliminating deformation incompatibility in composites by gradient nanolayer architectures. *Sci. Rep.* **8**, 16216 (2018).
48. Hofmann, D. C. et al. Developing gradient metal alloys through radial deposition additive manufacturing. *Sci. Rep.* **4**, 5357 (2014).
49. Tan, X. P. et al. Graded microstructure and mechanical properties of additive manufactured Ti–6Al–4V via electron beam melting. *Acta Mater.* **97**, 1–16 (2015).
50. Estrin, Y. & Vinogradov, A. Extreme grain refinement by severe plastic deformation: a wealth of challenging science. *Acta Mater.* **61**, 782–817 (2013).
51. Wang, K., Tao, N. R., Liu, G., Lu, J. & Lu, K. Plastic strain-induced grain refinement at the nanometer scale in copper. *Acta Mater.* **54**, 5281–5291 (2006).
52. Tao, N. R. & Lu, K. Nanoscale structural refinement via deformation twinning in face-centered cubic metals. *Scr. Mater.* **60**, 1039–1043 (2009).
53. Lu, K. Making strong nanomaterials ductile with gradients. *Science* **345**, 1455–1456 (2014).
54. Wu, X. L. et al. Heterogeneous lamella structure unites ultrafine-grain strength with coarse-grain ductility. *Proc. Natl Acad. Sci. USA* **112**, 14501–14505 (2015).
55. Chen, A. Y., Liu, J. B., Wang, H. T., Lu, J. & Wang, Y. M. Gradient twinned 304 stainless steels for high strength and high ductility. *Mater. Sci. Eng. A* **667**, 179–188 (2016).
56. Liu, Y. & Wei, Y. J. Gradient driven anomalous reversible plasticity in conventional magnesium alloys. *Extreme Mech. Lett.* **9**, 158–164 (2016).
57. Moering, J. et al. Synergetic strengthening far beyond rule of mixtures in gradient structured aluminum rod. *Scr. Mater.* **122**, 106–109 (2016).
58. Wu, X. L., Yang, M. X., Yuan, F. P., Chen, L. & Zhu, Y. T. Combining gradient structure and TRIP effect to produce austenite stainless steel with high strength and ductility. *Acta Mater.* **112**, 337–346 (2016).
59. Chen, L., Yuan, F. P., Jiang, P., Xie, J. J. & Wu, X. L. Mechanical properties and deformation mechanism of Mg-Al-Zn alloy with gradient microstructure in grain size and orientation. *Mater. Sci. Eng. A* **694**, 98–109 (2017).
60. Wang, Y. et al. Optimal stress and deformation partition in gradient materials for better strength and tensile ductility: a numerical investigation. *Sci. Rep.* **7**, 10954 (2017).
61. Fu, Z. Q. et al. Engineering heterostructured grains to enhance strength in a single-phase high-entropy alloy with maintained ductility. *Mater. Res. Lett.* **6**, 634–640 (2018).
62. Han, Z. H., Liang, S., Yang, J., Wei, R. & Zhang, C. J. A superior combination of strength-ductility in CoCrFeNiMn high-entropy alloy induced by asymmetric rolling and subsequent annealing treatment. *Mater. Charact.* **145**, 619–626 (2018).
63. Huang, C. X. et al. Interface affected zone for optimal strength and ductility in heterogeneous laminate. *Mater. Today* **21**, 713–719 (2018).
64. Ma, Z. W. et al. Cryogenic temperature toughening and strengthening due to gradient phase structure. *Mater. Sci. Eng. A* **712**, 358–364 (2018).
65. Wang, Y. F., Huang, C. X., Wang, M. S., Li, Y. S. & Zhu, Y. T. Quantifying the synergetic strengthening in gradient material. *Scr. Mater.* **150**, 22–25 (2018).
66. Yuan, F. P. et al. Ductility by shear band delocalization in the nano-layer of gradient structure. *Mater. Res. Lett.* **7**, 12–17 (2018).
67. Niu, G., Wu, H. B., Zhang, D., Gong, N. & Tang, D. Heterogeneous nano/ultrafine-grained medium Mn austenitic stainless steel with high strength and ductility. *Mater. Sci. Eng. A* **725**, 187–195 (2018).
68. Cheng, Z. & Lu, L. The effect of gradient order on mechanical behaviors of gradient nanotwinned Cu. *Scr. Mater.* **164**, 130–134 (2019).
69. Lee, H. H., Yoon, J. I., Park, H. K. & Kim, H. S. Unique microstructure and simultaneous enhancements of strength and ductility in gradient-microstructured Cu sheet produced by single-roll angular-rolling. *Acta Mater.* **166**, 638–649 (2019).
70. Wu, S. W. et al. Enhancement of strength-ductility trade-off in a high-entropy alloy through a heterogeneous structure. *Acta Mater.* **165**, 444–458 (2019).
71. Zhu, L. L. et al. Static and dynamic mechanical behaviors of gradient-nanotwinned stainless steel with a composite structure: experiments and modeling. *Int. J. Plast.* **114**, 272–288 (2019).
72. Long, Q. Y., Lu, J. X. & Fang, T. H. Microstructure and mechanical properties of AISI 316L steel with an inverse gradient nanostructure fabricated by electro-magnetic induction heating. *Mater. Sci. Eng. A* **751**, 42–50 (2019).
73. Wu, X. L. & Zhu, Y. T. Heterogeneous materials: a new class of materials with unprecedented mechanical properties. *Mater. Res. Lett.* **5**, 527–532 (2017).
74. Ding, J. et al. Mechanical behavior of structurally gradient nickel alloy. *Acta Mater.* **149**, 57–67 (2018).
75. Zhou, X., Li, X. Y. & Lu, K. Strain hardening in gradient nano-grained Cu at 77K. *Scr. Mater.* **153**, 6–9 (2018).
76. Bian, X. D., Yuan, F. P., Zhu, Y. T. & Wu, X. L. Gradient structure produces superior dynamic shear properties. *Mater. Res. Lett.* **5**, 501–507 (2017).
77. Shao, C. W. et al. Simultaneous improvement of strength and plasticity: additional work-hardening from gradient microstructure. *Acta Mater.* **145**, 413–428 (2018).
78. Zhang, P. & Lindemann, J. Influence of shot peening on high cycle fatigue properties of the high-strength wrought magnesium alloy AZ80. *Scr. Mater.* **52**, 485–490 (2005).
79. Liu, W. C. et al. Improvement of fatigue properties by shot peening for Mg–10Gd–3Y alloys under different conditions. *Mater. Sci. Eng. A* **528**, 5935–5944 (2011).
80. Nazari, A. Modeling fracture toughness of ferritic and austenitic functionally graded steel based on the strain gradient plasticity theory. *Comp. Mater. Sci.* **50**, 3238–3244 (2011).
81. Nielsen, K. L., Niordson, C. F. & Hutchinson, J. W. Strain gradient effects on steady state crack growth in rate-sensitive materials. *Eng. Fract. Mech.* **96**, 61–71 (2012).
82. Trudel, A., Lévesque, M. & Brochu, M. Microstructural effects on the fatigue crack growth resistance of a stainless steel CA6NM weld. *Eng. Fract. Mech.* **115**, 60–72 (2014).
83. Zhang, K., Wang, Z. B. & Lu, K. Enhanced fatigue property by suppressing surface cracking in a gradient nanostructured bearing steel. *Mater. Res. Lett.* **5**, 258–266 (2016).
84. Pandey, V., Chattopadhyay, K., Santhi Srinivas, N. C. & Singh, V. Role of ultrasonic shot peening on low cycle fatigue behavior of 7075 aluminium alloy. *Int. J. Fatigue* **103**, 426–435 (2017).
85. Zhang, S. J. et al. Fatigue crack growth behavior in gradient microstructure of hardened surface layer for an axle steel. *Mater. Sci. Eng. A* **700**, 66–74 (2017).
86. Zhou, J., Sun, Z., Kanouté, P. & Retraint, D. Effect of surface mechanical attrition treatment on low cycle fatigue properties of an austenitic stainless steel. *Int. J. Fatigue* **103**, 309–317 (2017).
87. Giang, N. A., Seupel, A., Kuna, M. & Hütter, G. Dislocation pile-up and cleavage: effects of strain gradient plasticity on micro-crack initiation in ferritic steel. *Int. J. Fract.* **214**, 1–15 (2018).
88. Martínez-Pañeda, E., Deshpande, V. S., Niordson, C. F. & Fleck, N. A. The role of plastic strain gradients in the crack growth resistance of metals. *J. Mech. Phys. Solids* **126**, 136–150 (2019).
89. Wang, Y. et al. The influence of combined gradient structure with residual stress on crack-growth behavior in medium carbon steel. *Eng. Fract. Mech.* **209**, 369–381 (2019).
90. Long, J. Z., Pan, Q. S., Tao, N. R. & Lu, L. Residual stress induced tension-compression asymmetry of gradient nanograined copper. *Mater. Res. Lett.* **6**, 456–461 (2018).
91. Lei, Y. B., Wang, Z. B., Xu, J. L. & Lu, K. Simultaneous enhancement of stress- and strain-controlled fatigue properties in 316L stainless steel with gradient nanostructure. *Acta Mater.* **168**, 133–142 (2019).
92. Zhang, Y. S., Han, Z., Wang, K. & Lu, K. Friction and wear behaviors of nanocrystalline surface layer of pure copper. *Wear* **260**, 942–948 (2006).
93. Prakash, N. A., Gnanamoorthy, R. & Kamaraj, M. Friction and wear behavior of surface nanocrystallized aluminium alloy under dry sliding condition. *Mater. Sci. Eng. B* **168**, 176–181 (2010).
94. Amanov, A., Lee, S. W. & Pyun, Y. S. Low friction and high strength of 316L stainless steel tubing for biomedical applications. *Mater. Sci. Eng. C.* **71**, 176–185 (2017).
95. Bernoulli, D., Cao, S. C., Lu, J. & Dao, M. Enhanced repeated frictional sliding properties in 304 stainless steel with a gradient nanostructured surface. *Surf. Coat. Technol.* **339**, 14–19 (2018).
96. Ge, M. Z. et al. Wear behavior of Mg-3Al-1Zn alloy subjected to laser shock peening. *Surf. Coat. Technol.* **337**, 501–509 (2018).
97. Balusamy, T. et al. Influence of surface mechanical attrition treatment (SMAT) on the corrosion behaviour of AISI 304 stainless steel. *Corros. Sci.* **74**, 332–344 (2013).
98. Hao, Y., Deng, B., Zhong, C., Jiang, Y. & Li, J. Effect of surface mechanical attrition treatment on corrosion behavior of 316 stainless steel. *J. Iron Steel Res. Int.* **16**, 68–72 (2009).

99. Li, N. N., Shi, S. Q., Luo, J. L., Lu, J. & Wang, N. Effects of surface nanocrystallization on the corrosion behaviors of 316L and alloy 690. *Surf. Coat. Technol.* **309**, 227–231 (2017).
100. Meyers, M. A., Mishra, A. & Benson, D. J. Mechanical properties of nanocrystalline materials. *Prog. Mater. Sci.* **51**, 427–556 (2006).
101. Lu, L., Shen, Y., Chen, X., Qian, L. & Lu, K. Ultrahigh strength and high electrical conductivity in copper. *Science* **304**, 422–426 (2004).
102. Lu, L., Chen, X., Huang, X. & Lu, K. Revealing the maximum strength in nano-twinned copper. *Science* **323**, 607–610 (2009).
103. Anderoglu, O. et al. Epitaxial nanotwinned Cu films with high strength and high conductivity. *Appl. Phys. Lett.* **93**, 083108 (2008).
104. Bufford, D., Wang, H. & Zhang, X. High strength, epitaxial nanotwinned Ag films. *Acta Mater.* **59**, 93–101 (2011).
105. Idrissi, H., Wang, B., Colla, M. S. & Raskin, J. P. Ultrahigh strain hardening in thin palladium films with nanoscale twins. *Adv. Mater.* **23**, 2119–2122 (2011).
106. Wang, Y. M. et al. Defective twin boundaries in nanotwinned metals. *Nat. Mater.* **12**, 697–702 (2013).
107. Li, Q. et al. High-strength nanotwinned Al alloys with 9R phase. *Adv. Mater.* **30**, 1704629 (2018).
108. Jang, D., Li, X., Gao, H. & Greer, J. R. Deformation mechanisms in nanotwinned metal nanopillars. *Nat. Nanotechnol.* **7**, 594–601 (2012).
109. Zhu, T., Li, J., Samanta, A., Kim, H. G. & Suresh, S. Interfacial plasticity governs strain rate sensitivity and ductility in nanostructured metals. *Proc. Natl Acad. Sci. USA* **104**, 3031–3036 (2007).
110. Li, X., Wei, Y., Lu, L., Lu, K. & Gao, H. Dislocation nucleation governed softening and maximum strength in nano-twinned metals. *Nature* **464**, 877–880 (2010).
111. You, Z. et al. Plastic anisotropy and associated deformation mechanisms in nanotwinned metals. *Acta Mater.* **61**, 217–227 (2013).
112. Pan, Q., Zhou, H., Lu, Q., Gao, H. & Lu, L. History-independent cyclic response of nanotwinned metals. *Nature* **551**, 214–217 (2017).
113. Zhou, H., Li, X., Qu, S., Yang, W. & Gao, H. A jogged dislocation governed strengthening mechanism in nanotwinned metals. *Nano Lett.* **14**, 5075–5080 (2014).
114. Zhou, H., Qu, S. & Yang, W. Toughening by nano-scaled twin boundaries in nanocrystals. *Model. Simul. Mater. Sci. Eng.* **18**, 065002 (2010).
115. Sansoz, F., Lu, K., Zhu, T. & Misra, A. Strengthening and plasticity in nanotwinned metals. *MRS Bull.* **41**, 292–297 (2016).
116. Sun, L., He, X. & Lu, J. Nanotwinned and hierarchical nanotwinned metals: a review of experimental, computational and theoretical efforts. *npj Comp. Mater.* **4**, 6 (2018).
117. Qu, S. et al. Microstructural evolution and mechanical properties of Cu–Al alloys subjected to equal channel angular pressing. *Acta Mater.* **57**, 1586–1601 (2009).
118. Zhang, Z. et al. Dislocation mechanisms and 3D twin architectures generate exceptional strength-ductility-toughness combination in CrCoNi medium entropy alloy. *Nat. Commun.* **8**, 14390 (2017).
119. Kou, H. N., Lu, J. & Li, Y. High-strength and high-ductility nanostructured and amorphous metallic materials. *Adv. Mater.* **26**, 5518–5524 (2014).
120. Yuan, F. P. & Wu, X. L. Size effects of primary/secondary twins on the atomistic deformation mechanisms in hierarchically nanotwinned metals. *J. Appl. Phys.* **113**, 203516 (2013).
121. Yuan, F. P. & Wu, X. L. Atomistic scale fracture behaviours in hierarchically nanotwinned metals. *Philos. Mag.* **93**, 3248–3259 (2013).
122. Yuan, F. P., Chen, L., Jiang, P. & Wu, X. L. Twin boundary spacing effects on shock response and spall behaviors of hierarchically nanotwinned fcc metals. *J. Appl. Phys.* **115**, 063509 (2014).
123. Hart, E. W. Theory of the tensile test. *Acta Metall.* **15**, 351–355 (1967).
124. Hutchinson, J. W. & Neale, K. W. Influence of strain-rate sensitivity on necking under uniaxial tension. *Acta Metall.* **25**, 839–846 (1977).
125. Yasnikov, I. S., Vinogradov, A. & Estrin, Y. Revisiting the Considère criterion from the viewpoint of dislocation theory fundamentals. *Scr. Mater.* **76**, 37–40 (2014).
126. Gupta, R. K. & Birbilis, N. The influence of nanocrystalline structure and processing route on corrosion of stainless steel: a review. *Corros. Sci.* **92**, 1–15 (2015).
127. Lu, K. Stabilizing nanostructures in metals using grain and twin boundary architectures. *Nat. Rev. Mater.* **1**, 16019 (2016).
128. Zhao, J. et al. Multiple mechanism based constitutive modeling of gradient nanograined material. *Inter. J. Plast.* **125**, 314–330 (2019).
129. Yang, M. et al. Residual stress provides significant strengthening and ductility in gradient structured materials. *Mater. Res. Lett.* **7**, 433–438 (2019).
130. Zhu, Y. & Wu, X. Perspective on hetero-deformation induced (HDI) hardening and back stress. *Mater. Res. Lett.* **7**, 393–398 (2019).
131. Evans, A. G. & Hutchinson, J. W. A critical assessment of theories of strain gradient plasticity. *Acta Mater.* **57**, 1675–1688 (2009).
132. Fleck, N. A., Muller, G. M., Ashby, M. F. & Hutchinson, J. W. Strain gradient plasticity-theory and experiment. *Acta Metall. Mater.* **42**, 475–487 (1994).
133. Nix, W. D. & Gao, H. J. Indentation size effects in crystalline materials: a law for strain gradient plasticity. *J. Mech. Phys. Solids* **46**, 411–425 (1998).
134. Ashby, M. F. The deformation of plastically non-homogeneous materials. *Phil. Mag.* **21**, 399–424 (1970).
135. Gao, H., Huang, Y., Nix, W. D. & Hutchinson, J. W. Mechanism-based strain gradient plasticity-I. Theory. *J. Mech. Phys. Solids* **47**, 1239–1263 (1999).
136. Huang, Y., Gao, H., Nix, W. D. & Hutchinson, J. W. Mechanism-based strain gradient plasticity-II. Analysis. *J. Mech. Phys. Solids* **48**, 99–128 (2000).
137. Cao, P. The strongest size in gradient nanograined metals. *Nano Lett.* **20**, 1440–1446 (2020).
138. Liu, Y., Bufford, D., Wang, H., Sun, C. & Zhang, X. Mechanical properties of highly textured Cu/Ni multilayers. *Acta Mater.* **59**, 1924–1933 (2011).
139. Wang, J., Beyerlein, I. J., Mara, N. A. & Bhattacharyya, D. Interface-facilitated deformation twinning in copper within submicron Ag–Cu multilayered composites. *Scr. Mater.* **64**, 1083–1386 (2011).
140. Bufford, D., Bi, Z., Jia, Q. X., Wang, H. & Zhang, X. Nanotwins and stacking faults in high-strength epitaxial Ag/Al multilayer films. *Appl. Phys. Lett.* **101**, 223112 (2012).
141. Zheng, S. et al. High strength and thermal stability due to twin-induced interfaces. *Nat. Commun.* **4**, 1696 (2013).
142. Zheng, S. et al. Plastic instability mechanisms in bimetallic nanolayered composites. *Acta Mater.* **79**, 282–291 (2014).
143. Wang, J. & Misra, A. An overview of interface-dominated deformation mechanisms in metallic multilayers. *Curr. Opin. Solid State Mater. Sci.* **15**, 20–28 (2011).
144. Wang, J., Zhou, Q., Shao, S. & Misra, A. Strength and plasticity of nanolaminated materials. *Mater. Res. Lett.* **5**, 1–19 (2017).
145. Regueiro, R. A., Bammann, D. J., Marin, E. B. & Garikipati, K. A nonlocal phenomenological anisotropic finite deformation plasticity model accounting for dislocation defects. *J. Eng. Mater. Technol.* **124**, 380–387 (2002).
146. Shizawa, K. & Zbib, H. M. A thermodynamical theory of gradient elastoplasticity with dislocation density tensor. I: fundamentals. *Int. J. Plast.* **15**, 899–938 (1999).
147. Yefimov, S., Groma, I. & van der Giessen, E. A comparison of a statistical-mechanics based plasticity model with discrete dislocation plasticity calculations. *J. Mech. Phys. Solids* **52**, 279–300 (2004).
148. Han, C. S., Gao, H., Huang, Y. & Nix, W. D. Mechanism-based strain gradient crystal plasticity. I. Theory. *J. Mech. Phys. Solids* **53**, 1188–1203 (2005).
149. Bayley, C. J., Brekelmans, W. A. M. & Geers, M. G. D. A comparison of dislocation induced back stress formulations in strain gradient crystal plasticity. *Int. J. Solids Struct.* **43**, 7268–7286 (2006).
150. Winning, M., Gottstein, G. & Shvindlerman, L. S. Stress induced grain boundary motion. *Acta Mater.* **49**, 211–219 (2001).
151. Cahn, J. W., Mishin, Y. & Suzuki, A. Coupling grain boundary motion to shear deformation. *Acta Mater.* **54**, 4953–4975 (2006).
152. Rupert, T. J., Gianola, D. S., Gan, Y. & Hemker, K. J. Experimental observations of stress-driven grain boundary migration. *Science* **326**, 1686–1690 (2009).
153. Gottstein, G. & Molodov, D. A. Grain boundary migration in metals: recent developments. *Inter. Sci.* **6**, 7–22 (1998).
154. Zhou, X., Li, X. & Lu, K. Size dependence of grain boundary migration in metals under mechanical loading. *Phys. Rev. Lett.* **122**, 12601 (2019).
155. Pilania, G., Wang, C., Jiang, X., Rajasekaran, S. & Ramprasad, R. Accelerating materials property predictions using machine learning. *Sci. Rep.* **3**, 2810 (2013).
156. Meredig, B. et al. Combinatorial screening for new materials in unconstrained composition space with machine learning. *Phys. Rev. B* **89**, 094104 (2014).
157. Raccugli, P. et al. Machine-learning-assisted materials discovery using failed experiments. *Nature* **533**, 73–76 (2016).
158. Butler, K. T., Davies, D. W., Cartwright, H., Isayev, O. & Walsh, A. Machine learning for molecular and materials science. *Nature* **559**, 547–555 (2018).
159. Wu, G. et al. Hierarchical nanostructured aluminum alloy with ultrahigh strength and large plasticity. *Nat. Commun.* **10**, 5099 (2019).
160. Wu, X. et al. Nanodomained nickel unite nanocrystal strength with coarse-grain ductility. *Sci. Rep.* **5**, 11728 (2015).
161. Xu, Y., Fu, Y. & Chen, H. Planar gradient metamaterials. *Nat. Rev. Mater.* **1**, 16067 (2016).

Acknowledgements
The authors gratefully acknowledge financial support from the National Natural Science Foundation of China (grant no. 51420105001). H.G. has also received funding from the US National Science Foundation (grant no. DMR-1709318). L.L. thanks the National Natural Science Foundation of China (grant nos 51471172, 51931010 and U1608257), the Key Research Program of Frontier Sciences and the International Partnership Program (grant no. GJHZ2029) of the Chinese Academy of Sciences, and the LiaoNing Revitalization Talents Program (grant no. XLYC1802026). X.L. acknowledges financial support from the National Natural Science Foundation of China (grant nos 11522218 and 11720101002), the Beijing Natural Science Foundation (grant no. Z180014) and the National Science and Technology Major Project (grant no. 2017-VI-0003–0073).

Author contributions
X.L., L.L. and H.G. discussed the content. All authors contributed to the writing, reviewing and editing of the manuscript.

Competing interests
The authors declare no competing interests.

Publisher's note
Springer Nature remains neutral with regard to jurisdictional claims in published maps and institutional affiliations.